Chapter 2
Meso-Scale Modeling: The EMMS Model for Gas-Solid Systems

Abstract This chapter introduces the EMMS model for gas-solid two-phase flow and the motive for this series of work. The EMMS model focuses on the meso-scale phenomenon of particle clustering, correlating it to the micro-scale of single particles and the macro-scale of the vessel operating conditions, material properties, and boundary conditions by analyzing the compromise between dominant mechanisms to define the meso-scale stability condition. The EMMS model can be solved for the eight parameters that describe the meso-scale structure and capture the so-called choking and drag-reduction phenomena in gas-solid fluidization systems, and further enables the intrinsic regime, operation diagram and overall fluid dynamics of systems to be determined. This chapter provides a solid basis to integrate the EMMS model with computational fluid dynamics (CFD) simulations and develop the EMMS paradigm.

Keywords Choking · Cluster · Compromise · Drag · EMMS · Fluidization · Hydrodynamics · Meso-scale structure · Multiscale · Stability condition

Notation

a	Acceleration, m/s^2
C_b	Coefficient of added mass force, -
C_D	Drag coefficient for particles, -
C_{D0}	Drag coefficient for a single particle, -
d	Diameter, m
F	Gas-solid interaction, N
f	Volume fraction (of dense phase), -
$F_i(X)$	Conservation equation, -
g	Gravity acceleration, m/s^2
G_s	Solids flow rate, kg/(m^2·s)
H	Solids bed height, m
I	Solids inventory, kg

J. Li et al., *From Multiscale Modeling to Meso-Science*,
DOI: 10.1007/978-3-642-35189-1_2,

K	Proportional factor, -
K^*	Saturation carrying capacity, kg/(m^2·s)
m	Particle or cluster number in unit volume, m^{-3}
N	Rate of energy dissipation per unit mass of solids, m^2/s^3
P	Pressure, kPa
Q	Volume flow rate, m^3/s
r	Radial coordinate, m
R	Radius, m
Re	Reynolds number, -
t	Time, s
U	Superficial velocity, m/s
u	Velocity, m/s
W	Energy consumption with respect to unit volume, J/m^3 s
z	Axial coordinate, m
δ_b	Bubble holdup, -
v	Kinematic viscosity, m^2/s
ρ	Density, kg/m^3
σ	Variation of local solids concentration fluctuation, -
ε	Voidage, -
μ	Viscosity, Pa·s

Subscripts

*	Top dilute region
a	Bottom dense region
b	Bubble
c	Dense phase
cl	Cluster
d	Dissipation
e	Emulsion
f	Dilute phase, fluid
g	Gas
i	Interface
imp	Imposed pressure
max	Maximum
mb	Minimum bubbling
mf	Minimum fluidization
min	Minimum
p	Particle
pt	Value for choking point
s	Suspension, slip
T	Total
t	Transport, terminal
uni	Uniform

2.1 Background

2.1.1 Designation

If a gas passes upward through a bed of particles at very low velocity, the drag of the gas is not large enough to support the whole weight of the particles. For coarse particles, the gas-solid system remains in a fixed-bed state until the gas velocity reaches the minimum fluidization velocity U_{mf}, at which point the gas-solid system fluidizes, becoming particulate with particles uniformly distributed in the flowing gas. Above U_{mf}, the gas-solid system immediately becomes aggregative, as depicted in Fig. 2.1, forming a two-phase structure consisting of a discrete dilute phase of gas-rich bubbles and a continuous dense phase of solid-rich emulsion. For fine or graded powders, instead of a minimum fluidization state appearing, the gas-solid system remains particulate until the gas velocity gradually approaches the minimum bubbling velocity U_{mb}, at which point gas bubbles start to appear.

Some criteria to distinguish particulate from aggregative fluidization based on the Froude number have been proposed (Wilhelm and Kwauk 1948; Romero and Johanson 1962). However, distinguishing between these types of fluidization may be difficult if smooth or size-graded particles are used. If the gas velocity is high enough to alter the shape of the bubbles so that a new two-phase structure appears, then the gas-solid system enters a so-called "fast fluidization" regime and can be described as a circulating fluidized bed (CFB) (Reh 1971; Yerushalmi et al. 1976).

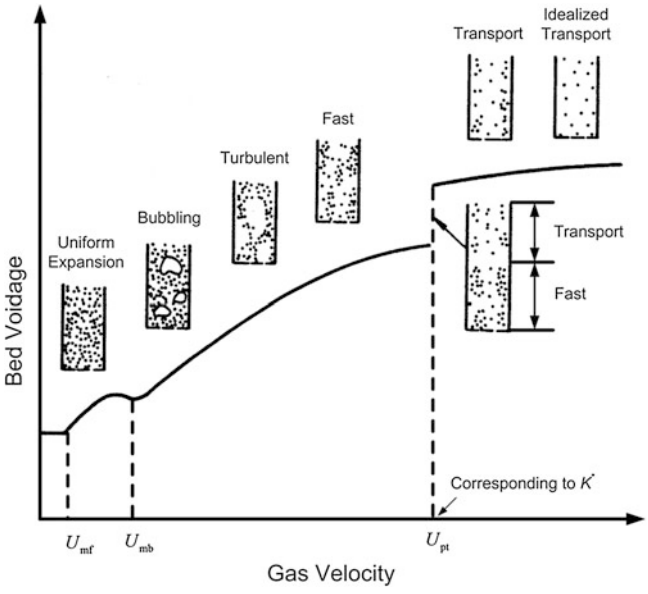

Fig. 2.1 Aggregative gas-solid two-phase flow (Li and Kwauk 1994)

In this regime, particle clusters are dispersed as a discontinuous phase in a dilute continuous phase. Phase inversion occurs between the bubbling and "fast" modes. However, this transition is diffuse and corresponds to what is often referred to as "turbulent fluidization" (Lanneau 1960) in aggregative fluidization, and is accompanied by large bubble deformation and simultaneous sporadic separation of the dense phase into initial clusters.

With a further increase in gas velocity, the fast fluidization regime suddenly terminates with the onset of dilute transport at transition velocity U_{pt}. This sudden reversion is characterized by a step change in voidage and bed structure. The highest solids circulation rate corresponding to this transition velocity is called the saturation carrying capacity K^*. At even higher gas velocities, ideal homogeneity becomes evident as particles begin to behave discretely.

The structure of the gas-solid two-phase flow changes with operating parameters and material properties. A specific phase structure could be confined to a fairly small region such as a bubble or cluster, or extended through much larger regions of the vessel. Kwauk and Li (1996) proposed a four category scheme to describe this complicated phenomenon:

- ***Phase:*** used to describe local heterogeneity resulting from differences in particle aggregation, such as the solid-rich dense phase and gas-rich dilute phase in gas-solid systems;
- ***Regime:*** used to describe the configuration of phase combinations dependent on operating parameters such as bubbling, turbulent, and fast fluidization regimes;
- ***Pattern:*** used to describe the constitution of the regime spectrum dependent on material properties, such as bubbling/transport for coarse gas-solid systems, particulate/bubbling/turbulent/fast/transport for fluid catalytic cracking (FCC) catalyst/air systems, and particulate for most liquid-solid systems;
- ***Region:*** used to describe the spatial distributions of phase, regime and pattern, from nearly homogeneous structures for liquid-solid systems to heterogeneous structures for gas-solid systems, depending on boundary conditions, such as top, bottom, core and wall regions.

This methodology is directed towards a comprehensive understanding of gas-solid two-phase flow, indicating the relationships between the above four categories and the three independent factors dominating the system—operating parameters, material properties, and boundary conditions.

2.1.2 Structural Characteristics

From the structural changes observed in gas-solid systems resulting from increasing gas velocity, the complexity of gas-solid systems is mainly characterized by structure heterogeneity, bifurcation, and state multiplicity (Li et al. 1996).

Local structure heterogeneity refers to coexistence of a gas-rich dilute phase and solid-rich dense phase. By carrying out multiple resolution and time series

reconstructions of local solid concentration signals from a cross-optical probe (Reh and Li 1991) in a CFB with an inner diameter (ID) of 90 mm containing FCC particles fluidized with air, Cui et al. (2000) quantitatively described the nonlinear dynamic behavior of heterogeneous flow structure in gas-solid fluidization. With the data given in Fig. 2.2, they found three kinds of irregular components including dilute and dense phases, and a dilute/dense alternating element with random characteristics, with a complicated evolution of probability density distributions depending on operating conditions. Starting from symmetric distributions at low superficial gas velocities (Fig. 2.2a0–a2), the bubbles gradually increase in size with increasing U_g. Some particles enter bubbles to form clusters as a result of the induced perturbation, causing the probability density to change from a single symmetric peak to two with asymmetric distribution, as seen in Fig. 2.2b0–b2 and c0–c2. As U_g increases further, both the dense and dilute phases gradually break up, leading to smaller clusters and bubbles. Therefore, the left peak becomes more intense, while the right peak becomes weaker until it eventually disappears (Fig. 2.2d0–d2). At even higher U_g, gas velocity has little effect on the asymmetric distributions for all three kinds of elements. It is clear that the two-phase structure exists in the whole spectrum of fluidization regimes because of the self-organization of both the fluid and particles; that is, self-organization of the fluid leads to the formation of the dilute phase, whereas that of the particles results in the dense phase.

Bifurcation is related to regime multiplicity, referring to inflective or step changes of the steady state at a critical point at which regime multiplicity occurs. The

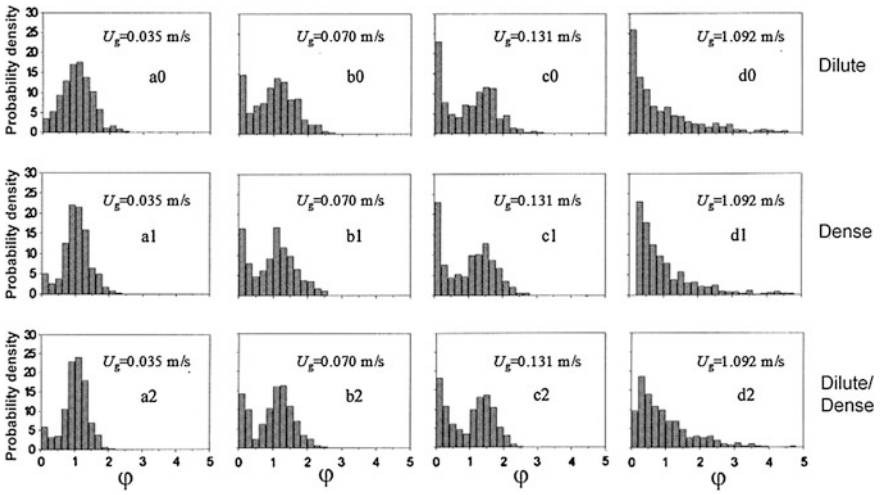

Fig. 2.2 Evolution of the probability density distributions of dilute and dense phases and the dilute/dense alternating element over time for different U_g in gas-solid systems (Cui et al. 2000) (φ is a non-dimensional irregular fluctuation coefficient). Reprinted from ref. Cui et al. (2000), Copyright 2012, with permission from Elsevier

first bifurcation generally occurs at U_{mb}, where a gas-solid system transitions from uniform expansion to bubbling fluidization. Then, the system suddenly segregates into dense emulsion and dilute bubble phases. With further increases in gas velocity, the system becomes more heterogeneous and forms dense cluster and dilute emulsion phases until another uniform structure (dilute transport) appears at U_{pt}. Engineers refer to this bifurcation as choking. The above behavior is also demonstrated in the bifurcation diagram of voidage versus fluid velocity presented in Fig. 2.3. The flow structure of the system is characterized by extreme behavior, showing the highest probabilities for the formation of the dense phase with voidage about the minimum fluidization voidage (ε_{mf}) and the dilute phase with voidage about 1.0. In the fixed-bed regime, bed voidage is consistently close to ε_{mf}. With the occurrence of the first bifurcation, an ordered two-phase structure appears, resulting in the alternating occurrence of the two extreme voidage values, ε_{mf} and 1.0. With increasing gas velocity, irregular disturbances appear and gradually intensify, as indicated by the increasing probability of voidage between these two extreme values. As soon as the second bifurcation occurs at U_{pt}, this extremum behavior ceases, and the distribution of voidage decreases to a narrow range.

State multiplicity represents simultaneous occurrence of top dilute and bottom dense steady states in a gas-solid fluidization system, or occurrence of either one under the same operating conditions, and requires the variational criterion to be identified to understand the prevailing steady state in a system. For any specified

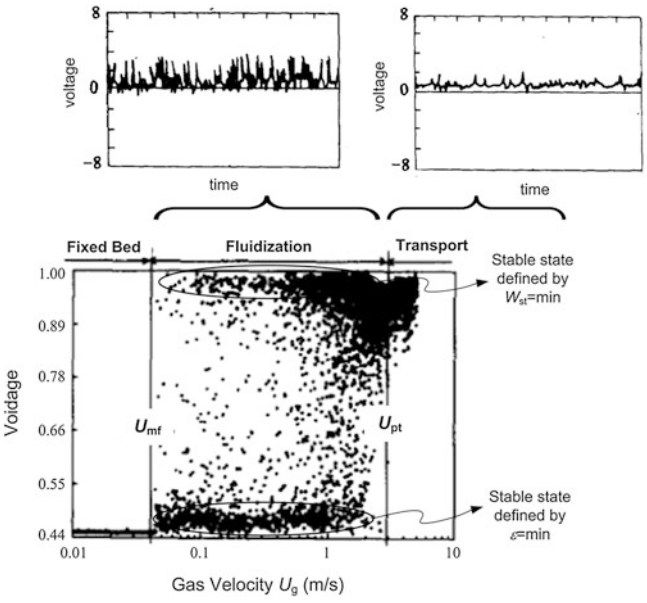

Fig. 2.3 Bifurcation diagram of local voidage measured by an optic probe (Li et al. 1996). Reprinted from ref. Li et al. (1996), Copyright 2012, with permission from Elsevier

operating conditions, the dense fluidization state in the bottom region cannot be distinguished from the dilute transport state at the top without analyzing stability because of the different variational criteria for these two states. Li et al. (1988a) studied the dependence of axial voidage profile on solids flow rate G_s, U_g and the imposed pressure drop ΔP_{imp} in a CFB with an ID of 90 mm using a scanning transducer valve system. Figure 2.4 shows the dependence of axial voidage profile on solid inventory I for FCC particles ($\rho_p = 929.5$ kg/m^3, $d_p = 54$ μm). The curves for $I = 15$ and 20 kg in Fig. 2.4a and $I = 15$, 20, and 22 kg in Fig. 2.4b are S-shaped, and contain two regions with a transition occurring inside the bed. Variation of I does not change the top or bottom voidage, but it does affect the position of the inflection point between the top dilute and bottom dense regions. On one hand, when I is increased, the inflection point will move up to the top of the bed so the axial voidage profile is no longer S-shaped, as shown by the curves in Fig. 2.4c and for $I = 25$, 35, and 40 kg in Fig. 2.4a and b. On the other hand, decreasing I causes the inflection point to move downward until the flow regime becomes dilute transport.

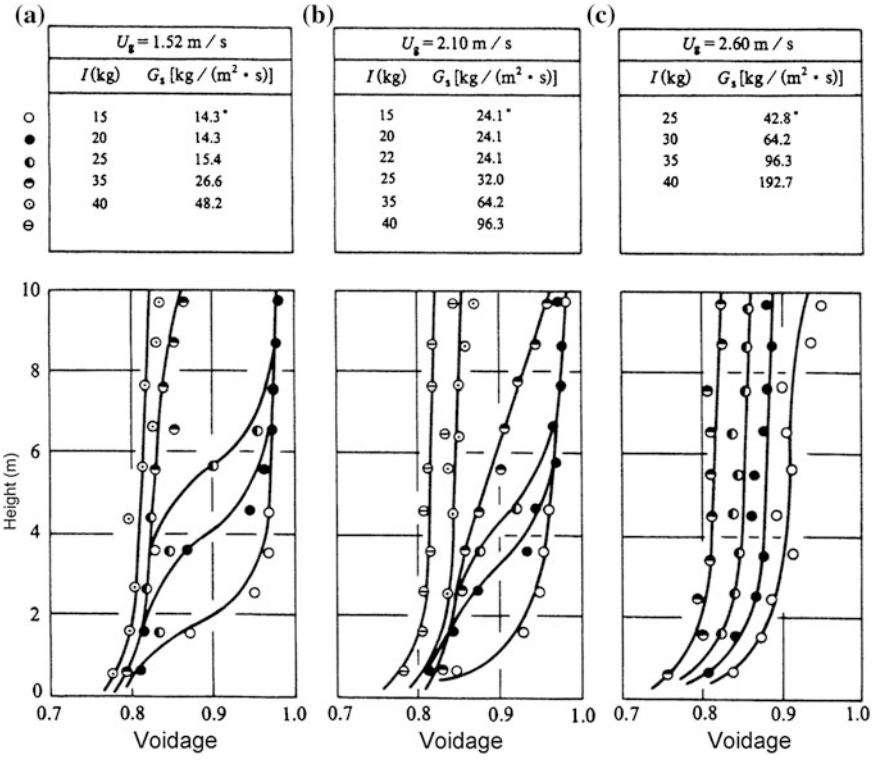

Fig. 2.4 Axial voidage profiles for a FCC catalyst/air system (Li et al. 1988a)

2.1.3 Modeling Methodology

As discussed above, gas-solid fluidization as a typical complex system is characterized by its spatio-temporal multiscale nature and forms dissipative structures through inherent nonlinear and non-equilibrium interactions. Challenges in quantitative design of gas-solid fluidization systems mainly arise from their complex two-phase heterogeneous structures, which result in different behaviors at different scales. There are three different approaches used to analyze multiscale heterogeneous structures:

- Tracking behaviors at the micro-scale to elucidate the details and mechanisms of complex systems;
- Averaging all parameters over a specific volume by considering the system to be uniform;
- Taking the multiscale structure into account and considering the disparity of behaviors and interactions at different scales.

Although commonly used, the averaging approach is not sufficient to characterize heterogeneous structures because it does not distinguish between different scales. However, the discrete approach based on micro-scale mechanisms is not yet practical because of the current limitations in measurement technology and computer capacity. Multiscale methodology is therefore a promising approach to cope with both stationary and dynamic structures. This approach, however, requires variational criteria to identify the prevailing steady state because the number of variables to be solved normally exceeds the available equations.

Multiscale methodology can be further classified into three types, descriptive, correlative and variational, as discussed in Chap. 1 (Li and Kwauk 2003). The variational multiscale method relates different relevant scales in multiscale structures. This method stipulates that (1) multiscale structures arise from the compromise between dominant mechanisms, and (2) the phenomena at different scales are determined by the stability condition of a given system. Therefore, the variational multiscale method focuses on revealing the relationship between phenomena on different scales and the overall behavior of the system by formulating the stability condition of the structure through analysis of the compromise between sub-mechanisms. Combination of the correlative and variational multiscale methods may produce a comprehensive approach to describe complex gas-solid systems. This will be discussed in Chap. 5, where the EMMS model is extended to the EMMS paradigm.

2.2 Formulation of the EMMS Model

2.2.1 Multiscale Analysis

The interaction between different dominant mechanisms (gas or solids) causes nonlinearity in gas-solid fluidization systems. The compromise between dominant mechanisms leads to the disparity of structures at different scales and spatio-temporal multiscale behaviors. Each dominant mechanism follows its own rule and extremum tendency. To understand multiscale structures and the interaction between different mechanisms, it is necessary to distinguish both dominant mechanisms and scale; that is, resolution with respect to both dominant mechanisms and scales is important and also the jumping-off point of this 3-decade research. Scale resolution is easily understood, as outlined in Fig. 2.5. Altogether eight parameters (ε_f, ε_c, f, U_f, U_c, U_{pf}, U_{pc}, and d_{cl}), as stated in Chap. 1, are needed to describe the state of a system, where ε_c, f, U_c, U_{pc} and d_{cl} describe the dense phase, and U_f, U_{pf} and ε_f explain the dilute one. The three scale interactions present in gas-solid fluidization systems are as follows:

- Micro-scale interaction between gas and solid is correlated with the size of the constituent particles and is present in both the dense and dilute phases. This

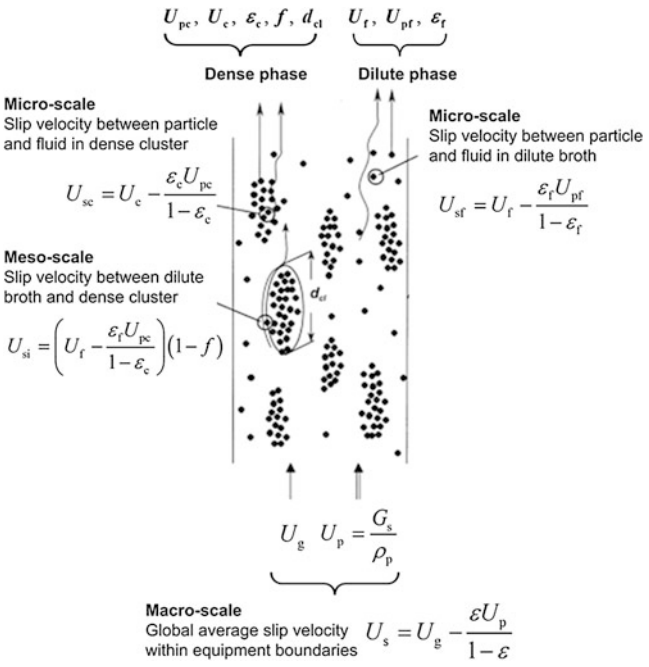

Fig. 2.5 Eight parameters and three scales of interaction in heterogeneous gas-solid flow (Li et al. 1999). Reprinted from ref. Li et al. (1999), Copyright 2012, with permission from Elsevier

interaction, expressed as the magnitude of the force acting on a single particle, can be written for the dense phase as:

$$F_{\mathrm{c}} = C_{\mathrm{Dc}} \frac{\pi d_{\mathrm{p}}^2}{4} \frac{\rho_{\mathrm{f}} U_{\mathrm{sc}}^2}{2}, \tag{2.1}$$

and for the dilute phase as:

$$F_{\mathrm{f}} = C_{\mathrm{Df}} \frac{\pi d_{\mathrm{p}}^2}{4} \frac{\rho_{\mathrm{f}} U_{\mathrm{sf}}^2}{2}. \tag{2.2}$$

- Meso-scale interaction between the dense clusters and dilute broth surrounding them is correlated with the size of bubbles or clusters. For particle clusters, this interaction is expressed as the magnitude of the force acting on a cluster by the broth through the so-called interface:

$$F_{\mathrm{i}} = C_{\mathrm{Di}} \frac{\pi d_{\mathrm{cl}}^2}{4} \frac{\rho_{\mathrm{f}} U_{\mathrm{si}}^2}{2}. \tag{2.3}$$

- Macro-scale interaction between the global gas-solid system and its boundaries is correlated with the size of the whole vessel in both the radial and axial directions. This interaction is fundamental to the dependence of meso-scale fluid dynamics on location.

U_{sc}, U_{sf}, and U_{si} are gas-solid slip velocities in the dense and dilute phases and the interface, respectively, and should be non-negative,

$$U_{\mathrm{sc}} = U_{\mathrm{c}} - \frac{\varepsilon_{\mathrm{c}} U_{\mathrm{pc}}}{1 - \varepsilon_{\mathrm{c}}} \geq 0, \tag{2.4}$$

$$U_{\mathrm{sf}} = U_{\mathrm{f}} - \frac{\varepsilon_{\mathrm{f}} U_{\mathrm{pf}}}{1 - \varepsilon_{\mathrm{f}}} \geq 0, \tag{2.5}$$

$$U_{\mathrm{si}} = \left(U_{\mathrm{f}} - \frac{\varepsilon_{\mathrm{f}} U_{\mathrm{pc}}}{1 - \varepsilon_{\mathrm{c}}} \right) (1 - f) \geq 0. \tag{2.6}$$

C_{Dc} and C_{Df} are drag coefficients for particles in the dense and dilute phases, respectively, and C_{Di} is that for particle clusters in the whole system. The drag coefficient C_{D0} for a single particle can be calculated for $Re_{\mathrm{p}} < 1000$ (Flemmer and Banks 1986) as

$$C_{\mathrm{D0}} = \frac{24}{Re_{\mathrm{p}}} + \frac{3.6}{Re_{\mathrm{p}}^{0.313}}, \tag{2.7}$$

and the drag coefficient for particles in homogeneous suspension such as particulate fluidization systems (Wen and Yu 1966) can be further calculated as

$$C_{\mathrm{D}} = C_{\mathrm{D0}} \varepsilon^{-4.7}. \tag{2.8}$$

Table 2.1 Definitions of the three drag coefficients for multiscale interactions

Parameter	Dense phase	Dilute phase	Interface
Reynolds number	$Re_c = U_{sc} d_p / \nu_f$	$Re_f = U_{sf} d_p / \nu_f$	$Re_i = U_{si} d_{cl} / \nu_f$
C_D for a single particle	$C_{D0c} = \frac{24}{Re_c} + \frac{3.6}{Re_c^{0.313}}$	$C_{D0f} = \frac{24}{Re_f} + \frac{3.6}{Re_f^{0.313}}$	$C_{D0i} = \frac{24}{Re_i} + \frac{3.6}{Re_i^{0.313}}$
C_D for fluidized particles	$C_{Dc} = C_{D0c} \varepsilon_c^{-4.7}$	$C_{Df} = C_{D0f} \varepsilon_f^{-4.7}$	$C_{Di} = C_{D0i}(1-f)^{-4.7}$

These three drag coefficients, used to calculate multiscale interactions between particles and fluid in heterogeneous fluidization systems, can be correlated as indicated in Table 2.1. This is because the dense and dilute phases can be considered uniform suspensions, so the whole system can thus be regarded as consisting of dense clusters dispersed in a broth of sparsely distributed discrete particles.

The energy consumption in a gas-solid fluidization system can be resolved into a suspension and transport subsystem and an energy dissipation subsystem. That is, the total energy (N_T) associated with a flowing gas-solid system, expressed as power per unit mass of solids is considered to consist of two parts (Fig. 2.6); one describes suspension and transport of particles (N_{st}), and the other includes particle collision, circulation, and acceleration (N_d). N_{st} can be further divided into dissipative energies for particle suspension (N_s) and transport (N_t); that is,

$$N_T = N_{st} + N_d = N_s + N_t + N_d. \tag{2.9}$$

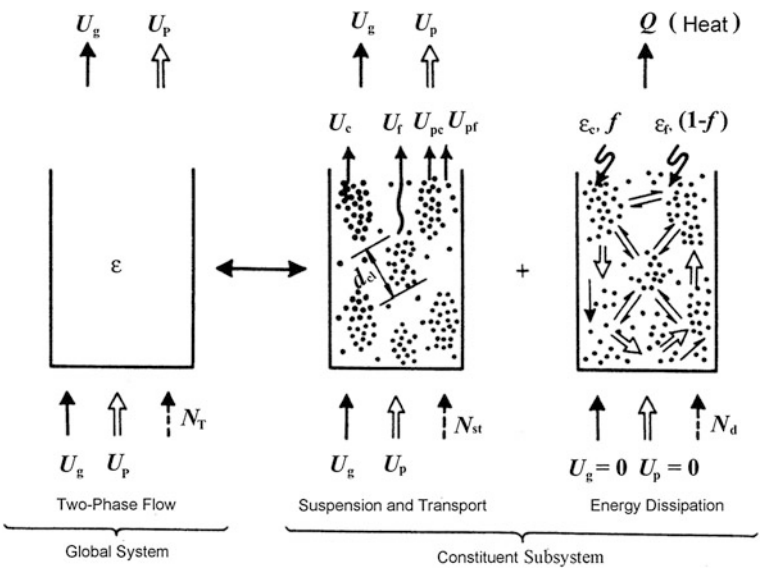

Fig. 2.6 System resolution for gas-solid fluidization systems (Li and Kwauk 1994)

Neglecting wall friction, the energy consumption per unit time equals the product of force and superficial gas velocity. The power per unit mass of solids can therefore be calculated as

$$N_{\mathrm{T}} = \frac{(\Delta P/\Delta L)U_{\mathrm{g}}}{(1-\varepsilon)\rho_{\mathrm{p}}} = \frac{(1-\varepsilon)\left(\rho_{\mathrm{p}}-\rho_{\mathrm{g}}\right)gU_{\mathrm{g}}}{(1-\varepsilon)\rho_{\mathrm{p}}} = \frac{\left(\rho_{\mathrm{p}}-\rho_{\mathrm{g}}\right)}{\rho_{\mathrm{p}}}gU_{\mathrm{g}}. \tag{2.10}$$

The energy N_{t} required to transport a unit mass of particles in a unit area at a flow rate G_{s} can be written as

$$N_{\mathrm{t}} = \frac{\left(\rho_{\mathrm{p}}-\rho_{\mathrm{g}}\right)gU_{\mathrm{p}}}{(1-\varepsilon)\rho_{\mathrm{p}}}. \tag{2.11}$$

According to Fig. 2.6, two steps can be used to analyze the suspension and transport subsystem, as illustrated in Fig. 2.7. First, the whole subsystem is treated as a combination of the two phases interacting with each other through an interface: a dense phase with voidage ε_{c} and volume faction f, and a dilute phase with voidage ε_{f} and volume faction $(1-f)$. The overall fluid flow is split into two streams, $U_{\mathrm{c}}f$ through the dense phase and $U_{\mathrm{f}}(1-f)$ through the dilute phase, and the change in pressure caused by fluid flow in the two phases should be equal. Second, the interaction between the dense and dilute phases is considered to occur through an independent fictitious interphase between the clusters and surrounding broth. The energy consumed in the suspension and transport subsystem N_{st} is thereby resolved into three constituent terms as follows:

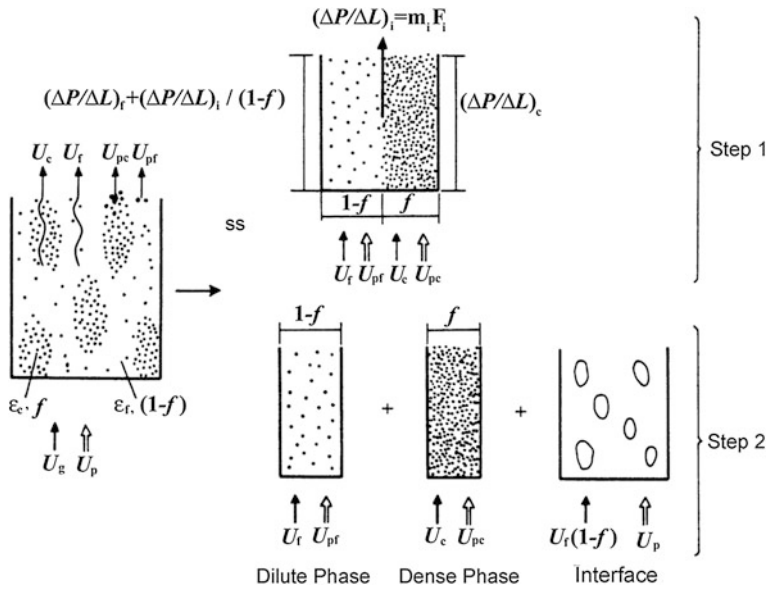

Fig. 2.7 Two-step resolution for the suspension and transport subsystem (Li and Kwauk 1994)

$$N_{\mathrm{st}} = (N_{\mathrm{st}})_{\mathrm{c}} + (N_{\mathrm{st}})_{\mathrm{f}} + (N_{\mathrm{st}})_{\mathrm{i}}, \tag{2.12}$$

each of which, in a similar manner to the power per unit mass of solids, can also be expressed as follows:

$$(N_{\mathrm{st}})_{\mathrm{c}} = \frac{f m_{\mathrm{c}}}{(1-\varepsilon)\rho_{\mathrm{p}}} F_{\mathrm{c}} U_{\mathrm{c}}, \tag{2.13}$$

$$(N_{\mathrm{st}})_{\mathrm{f}} = \frac{(1-f) m_{\mathrm{f}}}{(1-\varepsilon)\rho_{\mathrm{p}}} F_{\mathrm{f}} U_{\mathrm{f}}, \tag{2.14}$$

$$(N_{\mathrm{st}})_{\mathrm{i}} = \frac{m_{\mathrm{i}}}{(1-\varepsilon)\rho_{\mathrm{p}}} F_{\mathrm{i}} U_{\mathrm{f}} (1-f). \tag{2.15}$$

Therefore, N_{st} can be finally re-expressed as

$$\begin{aligned} N_{\mathrm{st}} &= \frac{1}{(1-\varepsilon)\rho_{\mathrm{p}}} \left[m_{\mathrm{c}} F_{\mathrm{c}} U_{\mathrm{c}} f + m_{\mathrm{f}} F_{\mathrm{f}} U_{\mathrm{f}} (1-f) + m_{\mathrm{i}} F_{\mathrm{i}} U_{\mathrm{f}} (1-f) \right] \\ &= \frac{3\rho_{\mathrm{f}}}{4(1-\varepsilon)\rho_{\mathrm{p}}} \left[\begin{array}{l} C_{\mathrm{Dc}} \dfrac{1-\varepsilon_{\mathrm{c}}}{d_{\mathrm{p}}} U_{\mathrm{sc}}^2 U_{\mathrm{c}} f + C_{\mathrm{Df}} \dfrac{1-\varepsilon_{\mathrm{f}}}{d_{\mathrm{p}}} U_{\mathrm{sf}}^2 U_{\mathrm{f}} (1-f) \\ + C_{\mathrm{Di}} \dfrac{f}{d_{\mathrm{cl}}} U_{\mathrm{si}}^2 U_f (1-f) \end{array} \right]. \end{aligned} \tag{2.16}$$

Energy consumption with respect to the unit volume of the reaction vessel W is used in the following analysis, and can be obtained by multiplying the energy consumption per unit mass of particles by the total mass of particles in the unit volume,

$$W_{\mathrm{T}} = N_{\mathrm{T}} (1-\varepsilon)\rho_{\mathrm{p}}, \tag{2.17}$$

$$W_{\mathrm{t}} = N_{\mathrm{t}} (1-\varepsilon)\rho_{\mathrm{p}}, \tag{2.18}$$

$$W_{\mathrm{st}} = N_{\mathrm{st}} (1-\varepsilon)\rho_{\mathrm{p}}. \tag{2.19}$$

It is worth noting that N_{st} characterizes the intrinsic tendency of particles to form an array with the lowest interaction with the fluid, whereas W_{st} represents the intrinsic tendency of the fluid to seek pathways with the lowest resistance to flow.

The resolution and multiscale analysis of gas-solid fluidization systems show that the multiscale gas-solid interactions in such systems can be quantified by the drag coefficients corresponding to the three subsystems of the dilute and dense phases and the interface. The momentum and mass conservation for the three subsystems make up the constitutive equations of the EMMS model.

2.2.2 Conservation Equations

Like other models, the EMMS model took a number of years to formulate, extend, and generalize. The original EMMS model is actually a zero-dimensional description of the time-averaged behavior of gas-solid fluidization based on a rather simplified physical picture:

- The gas-solid two-phase flow was considered to be one-dimensional, fully developed and independent of wall effects;
- The suspension was assumed to consist of a particle-rich dense phase composed of spherical clusters and a gas-rich dilute phase;
- Both the dilute and dense phases were considered to be uniform and stable.

Because fully developed flow was assumed, the drag acting on either particles or clusters was considered to be balanced by their respective effective gravities. However, this is not true when the model is applied to the elements in a two-fluid model (TFM) (Gidaspow 1994) because the particles or clusters are generally not in a hydrodynamic equilibrium state, but in continuous acceleration. Therefore, Ge and Li (2002) and Yang et al. (2003) extended the EMMS model so the accelerations of all particles in both dilute and dense phases could be calculated simultaneously. Further extension of the updated EMMS model accounted for the respective accelerations in the dense and dilute phases (Wang and Li 2007). With physical verification (Li et al. 2004; Zhang et al. 2005) and extension to different systems (Ge et al. 2007), the generality of the model has been recognized gradually, eventually leading to the EMMS paradigm for computation (Ge et al. 2011).

Although particle acceleration in both the dilute and dense phases has been taken into account in the updated EMMS model, the mathematical characteristics of the updated model are the same as those of the original. That is, altogether ten parameters (ε_f, ε_c, a_f, a_c, f, U_f, U_c, U_{pf}, U_{pc}, and d_{cl}) are needed to describe the state of a system, among which ε_c, a_c, f, U_c, U_{pc} and d_{cl} refer to the dense phase, and a_f, U_f, U_{pf} and ε_f to the dilute phase. However, the updated version of the EMMS model is also valid for sufficiently large areas in gas-solid systems where particle weight is not always equal to the drag acting on it, allowing spatio-temporal coupling of it with multiphase continuum models. By incorporating the structure-dependent drag coefficients calculated from the EMMS model to the TFM, the dynamic formation and dissolution of heterogeneous structures in concurrent-up gas-solid flow in a riser can be readily described, and the accuracy of the TFM is significantly improved compared with that using the Wen-Yu drag coefficient correlation (Yang et al. 2003; Wang and Li 2007).

It should be noted that the original EMMS model reveals the multiscale nature of gas-solid fluidization systems and functions as the basis of the updated model and EMMS paradigm even though it does not consider the effect of particle acceleration. More details about the original model can be found in the literature (Li and Kwauk 1994). This subsection will introduce in detail the conservation equations $F_i(X)$ used in the updated EMMS model.

1. ***Force balance equation for the dense phase***: the effective weight of a single cluster is equal to the sum of the forces exerted by the gas in both the dense and dilute phases,

$$m_c F_c f + m_i F_i = f(1-\varepsilon_c)(\rho_p - \rho_g)(g + a_c); \tag{2.20}$$

that is, substituting (2.1) and (2.3) yields conservation equation

$$\begin{aligned} &F_1(X) \\ &= \frac{3}{4} C_{Dc} \frac{f(1-\varepsilon_c)}{d_p} \rho_g U_{sc}^2 + \frac{3}{4} C_{Di} \frac{f}{d_{cl}} \rho_g U_{si}^2 - f(1-\varepsilon_c)\left(\rho_p - \rho_g\right)(g + a_c) \\ &= 0. \end{aligned} \tag{2.21}$$

2. ***Force balance equation for the dilute phase***: if both the gas and solids in the dense phase have no influence on particles in the dilute phase, the effective weight of particles in the dilute phase is equal to the force exerted by the gas in the dilute phase:

$$(1-f) m_f F_f = (1-f)(1-\varepsilon_f)\left(\rho_p - \rho_g\right)(g + a_f), \tag{2.22}$$

from which, on substituting (2.2), yields

$$\begin{aligned} &F_2(X) \\ &= \frac{3}{4} C_{Df} \frac{(1-f)(1-\varepsilon_f)}{d_p} \rho_g U_{sf}^2 - (1-f)(1-\varepsilon_f)\left(\rho_p - \rho_g\right)(g + a_f) = 0. \end{aligned} \tag{2.23}$$

3. ***Pressure balance equation***: the gas flow in the dilute phase has to support the discrete particles and clusters in suspension, and the combined forces result in a pressure gradient equal to that of the gas flow in the dense phase. The pressure gradient can be expressed as the product of the number density of particles and the drag on a single particle

$$m_f F_f + \frac{m_i F_i}{1-f} = m_c F_c; \tag{2.24}$$

that is, on substituting (2.2) and (2.3), gives

$$F_3(X) = C_{Df} \frac{1-\varepsilon_f}{d_p} \rho_g U_{sf}^2 + \frac{f}{1-f} C_{Di} \frac{1}{d_{cl}} \rho_g U_{si}^2 - C_{Dc} \frac{1-\varepsilon_c}{d_p} \rho_g U_{sc}^2 = 0. \tag{2.25}$$

4. ***Mass balance equation for the gas***: the net gas mass flow through the whole cross-section of the vessel should be equal to the sum of gas flow through both the dilute and dense phases:

$$F_4(X) = U_g - f U_c - (1-f) U_f = 0. \tag{2.26}$$

5. ***Mass balance equation for solid particles***: similar to the gas, the net solid mass flow through the whole cross-section of the vessel should be equal to the sum of mass flow through both the dilute and dense phases:

$$F_5(X) = U_p - fU_{pc} - (1-f)U_{pf} = 0. \tag{2.27}$$

6. ***Cluster diameter equation***: according to Chavan (1984), the diameter of a cluster (d_{cl}) can be assumed to be inversely proportional to the rate of energy input because the cluster diameter is generally greater than the size of energy dissipative vortices in gas-solid fluidization systems:

$$d_{cl} = \frac{K}{N_{input}}, \tag{2.28}$$

where N_{input} describes the separation of the dense phase into clusters; here K is a constant of proportionality. The cluster diameter is considered to be infinite at minimum fluidization, so the energy input at minimum fluidization $(N_{st})_{mf}$ should be subtracted from the total energy input, leading to

$$d_{cl} = \frac{K}{N_{st} - (N_{st})_{mf}}, \tag{2.29}$$

where

$$(N_{st})_{mf} = \frac{(\Delta P/\Delta L)_{mf}(U_g)_{mf}}{(1-\varepsilon_{mf})\rho_p} = \frac{(\rho_p - \rho_f)}{\rho_p}\left(U_{mf} + \frac{U_p\varepsilon_{mf}}{1-\varepsilon_{mf}}\right)g. \tag{2.30}$$

At a high enough gas velocity when the voidage reaches a specified value ε_{max}, all clusters separate into discrete particles. Matsen (1982) determined this voidage to be 0.9997 for fine particles, at which the cluster diameter equals the particle diameter, and N_{st} is almost completely consumed by particle transport with hardly any energy dissipated. This means N_s and N_d can both be neglected, hence

$$N_{st} \approx N_t; \tag{2.31}$$

that is,

$$(N_{st})|_{\varepsilon=\varepsilon_{max}} \approx (N_t)|_{\varepsilon=\varepsilon_{max}} = \frac{\rho_p - \rho_g}{\rho_p}\frac{gU_p}{1-\varepsilon_{max}}. \tag{2.32}$$

Thus, we get

$$K = gd_p\frac{\rho_p - \rho_g}{\rho_p}\left[\frac{U_p}{1-\varepsilon_{max}} - \left(U_{mf} + \frac{\varepsilon_{mf}U_p}{1-\varepsilon_{mf}}\right)\right], \tag{2.33}$$

which leads to the conservation equation

$$F_6(X) = d_{\mathrm{cl}} - \frac{g d_{\mathrm{p}} \left[\frac{U_{\mathrm{p}}}{1-\varepsilon_{\max}} - \left(U_{\mathrm{mf}} + \frac{\varepsilon_{\mathrm{mf}} U_{\mathrm{p}}}{1-\varepsilon_{\mathrm{mf}}} \right) \right]}{N_{\mathrm{st}} \frac{\rho_{\mathrm{p}}}{\rho_{\mathrm{p}} - \rho_{\mathrm{g}}} - \left(U_{\mathrm{mf}} + \frac{U_{\mathrm{p}} \varepsilon_{\mathrm{mf}}}{1-\varepsilon_{\mathrm{mf}}} \right) g} = 0. \tag{2.34}$$

Note that Eq. (2.34) appears only to be valid for systems with relatively high solid flux because in reactors with low solid flux such as CFB boilers the expression produces a cluster diameter smaller than the particle diameter. In fact, Eq. (2.34) predicts a cluster diameter larger than the particle diameter only if the energy input is greater than zero. Thus Lu et al. (2012) suggested the following modified cluster equation for hydrodynamic simulations of low solid fluxes,

$$d_{\mathrm{cl}} = d_{\mathrm{p}} \frac{\max\left((N_{\mathrm{t}})|_{\varepsilon=\varepsilon_{\max}}, (N_{\mathrm{st}})|_{\varepsilon=\varepsilon_{\max}} \right)}{\max(N_{\mathrm{st}}, N_{\mathrm{t}})}. \tag{2.35}$$

In gas-solid bubbling fluidized beds, the meso-scale structure is characterized by gas bubbles in place of particle clusters. Using an empirical bubble-size correlation to predict the maximum stable bubble diameter, Shi et al. (2011) proposed the EMMS/bubbling model. In this model, the states of the bubbling fluidized bed were resolved into emulsion and bubble phases with an interphase in between. Corresponding conservation equations were established based on force balance for particles in the emulsion and bubbles, mass balance for the gas and solids, and mean voidage and acceleration equations. The total mass-specific energy consumption rate was considered to be the sum of the energy dissipation rates in the emulsion phase and between the emulsion and bubble phases because the particle flow rate generally approaches zero in bubbling fluidized beds. The main formulae in the EMMS/bubbling model are summarized in Table 2.2.

It is clear that the conservation equations in terms of force balance and continuity in both the EMMS and EMMS/bubbling model are not sufficient to determine the fluid dynamics of a heterogeneous gas-solid fluidization system because

Table 2.2 Summary of the main formulae in the EMMS/bubbling model

Factor	Equation
Force balance for particles in the emulsion	$\frac{\pi d_{\mathrm{p}}^2}{8} C_{\mathrm{De}} \rho_{\mathrm{g}} U_{\mathrm{se}}^2 = \frac{\pi d_{\mathrm{p}}^3}{6} (\rho_{\mathrm{p}} - \rho_{\mathrm{g}})(g + a_{\mathrm{e}})$
Force balance for bubbles per unit volume	$\frac{\pi d_{\mathrm{b}}^2}{8} C_{\mathrm{Db}} \rho_{\mathrm{e}} U_{\mathrm{sb}}^2 = \frac{\pi d_{\mathrm{b}}^3}{6} (\rho_{\mathrm{e}} - \rho_{\mathrm{g}})(g + a_{\mathrm{b}})$
Mass balance for the gas	$U_{\mathrm{g}} - U_{\mathrm{ge}}(1 - \delta_{\mathrm{b}}) - U_{\mathrm{b}} \delta_{\mathrm{b}} = 0$
Mass balance for the solids	$U_{\mathrm{p}} - U_{\mathrm{pe}}(1 - \delta_{\mathrm{b}}) = 0$
Mean voidage equation	$\varepsilon = (1 - \delta_{\mathrm{b}})\varepsilon_{\mathrm{e}} + \delta_{\mathrm{b}}$
Acceleration equation[a]	$a_{\mathrm{b}} - a_{\mathrm{e}} = \frac{\sigma^2 (\rho_{\mathrm{p}} - \rho_{\mathrm{g}}) g}{C_{\mathrm{b}} (1-\varepsilon_{\mathrm{e}}) \delta_{\mathrm{b}} \rho_{\mathrm{e}}}$
Total energy consumption rate	$N_{\mathrm{st}} = \frac{3}{4} C_{\mathrm{De}} \frac{\rho_{\mathrm{g}}}{\rho_{\mathrm{p}}} \frac{U_{\mathrm{se}}^2}{d_{\mathrm{p}}} U_{\mathrm{ge}} = f_{\mathrm{b}} U_{\mathrm{g}} (g + a_{\mathrm{b}})$

[a] Zhang and Vanderheyden (2002)

the system is described by more independent variables than there are equations. An additional condition is needed to define the stable state of a gas-solid fluidization system; this is known as the stability condition.

2.2.3 Stability Condition

There is no common stability condition or general theory to describe nonlinear and non-equilibrium systems. Such systems are usually dominated by at least two mechanisms, each following a different tendency and having to compromise with the other. To establish and justify the stability condition of a system, the compromise between dominant mechanisms needs to be elucidated and then formulated as a relative extremum between the extreme tendencies of the dominant mechanisms.

In concurrent-up gas-solid two-phase flow, the gas tends to choose an upward path to minimize resistance, whereas particles tend to arrange themselves to minimize potential energy. Stability in a gas-solid two-phase system requires mutual compromise between gas and solid in following their respective tendencies. If the system is completely dominated by one, the intrinsic tendency of its dominant mechanism will be satisfied exclusively, with the total suppression of that for the other. However, when neither gas nor solid dominates, both have to compromise and concede their intrinsic tendency to that of the other to form a stable state.

If the gas velocity is lower than U_{mf}, the state of the gas-solid system is fixed-bed and becomes completely dominated by the particles or particle-dominating (PD). In this case, the intrinsic tendency of the particles is realized completely to reach minimal potential energy and the voidage tends to be minimized:

$$\varepsilon \rightarrow \min. \tag{2.36}$$

When the gas velocity falls within the range U_{mf} to U_{pt}, the system forms a fluidized bed where neither particles nor gas dominate exclusive realization of their tendency. The gas and particles have to compromise in such a way that the particles attempt to minimize potential energy and the gas flows through the system while trying to minimize resistance. This regime is called particle-fluid compromising (PFC), and is characterized by both minimal energy consumption for the gas and minimal voidage for the particles:

$$W_{\mathrm{st}} \rightarrow \min|_{\varepsilon \rightarrow \min}. \tag{2.37}$$

According to Eq. (2.19), the minimal energy consumption for the gas actually compromises with the minimal voidage for the particles. Thus, we can deduce that

$$N_{\mathrm{st}} = \frac{W_{\mathrm{st}}}{(1-\varepsilon)\rho_{\mathrm{p}}} \rightarrow \min \tag{2.38}$$

in the PFC regime.

At gas velocities greater than U_{pt}, all particles are transported in a dilute phase without forming clusters. Because particle clustering is suppressed by the high-velocity gas, this dilute homogeneous regime is fluid-dominating (FD). Under these conditions, the gas achieves the lowest resistance to gas flow by dispersing the particles as widely as possible, so

$$W_{st} \rightarrow \min. \tag{2.39}$$

According to the above analysis, it seems that the EMMS model correctly simulates gas-solid fluidization systems only if the fluidization regime is determined first. Li and Kwauk (1994) reflected that the energy dissipation resulting from particle-particle interactions in the FD regime tends to be minimal, thus leading to maximal energy consumption in the suspension and transport of particles. Therefore, a criterion to identify the transition from the PFC to the FD regime was established as follows:

$$(W_{st})_{PFC} \equiv (W_{st})_{(N_{st})_{min}} = (W_{st})_{(N_{st})_{max}}\big|_{\varepsilon=\varepsilon_{mf}} \equiv (W_{st})_{FD}. \tag{2.40}$$

Equation (2.40) defines the critical point at which the two-phase structure of dense fluidization separates into the uniform structure of dilute transport (Li et al. 1992). Accordingly, it is a suitable criterion to determine the choking point of a system, which will be discussed in detail in Sect. 2.3.3.

The existence of multiple regimes with distinctive flow structure is a remarkable characteristic of gas-solid fluidization. Ge and Li (2002) found that the minimization of N_{st} always requires the maximization of ε_f. Under these conditions, N_{st} does not always increase monotonically with ε_c; it may have, as depicted in Fig. 2.8, one local minimum at $\varepsilon_c = \varepsilon_{mf}$ and another at higher ε_c, denoted by ε_o. In this case, with the continuous variation of superficial gas velocity or solids circulation rate, there is a value where

$$N_{st}(\varepsilon_{mf}) = N_{st}(\varepsilon_o). \tag{2.41}$$

These two states are distinct, but they must coexist in a system. If this critical state is understood as choking with Eq. (2.41) being its criterion in place of Eq. (2.40), a more clear interpretation of choking appears, which is simply the shift between the two stable states. Thus,

$$N_{st} \rightarrow \min \tag{2.42}$$

can serve as a unified stability condition for all heterogeneous regimes in fluidization instead of taking separately Eqs. (2.38) and (2.39) as the respective stability conditions for the PFC and FD regimes. Zhang et al. (2005) verified this updated stability criterion through direct numerical simulation based on a pseudo-particle method. Results calculated based on the above simplification are in reasonable agreement with measurements obtained for bench, pilot and commercial scale CFBs.

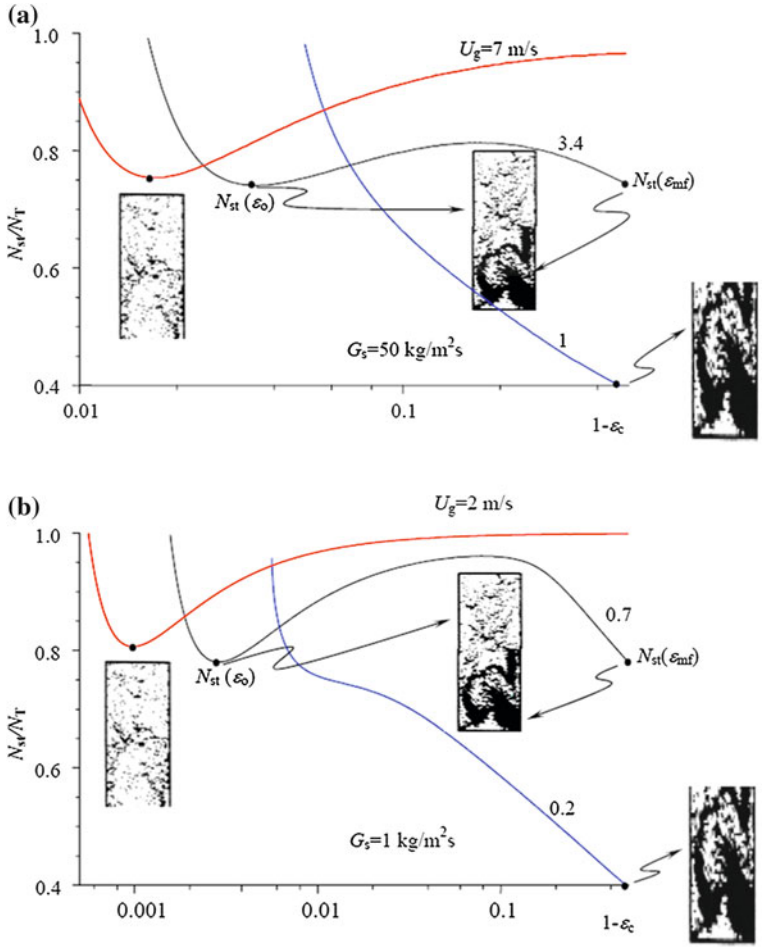

Fig. 2.8 Variation of N_{st} with ε_c in a typical gas-solid fluidization system with G_s of **a** 50 and **b** 1 kg/m^{2}s (Ge and Li 2002). Reprinted from ref. Ge and Li (2002), Copyright 2012, with permission from Elsevier

When U_g is less than U_{mf} or G_s is too high when $U_g > U_{mf}$, the gas flow does not provide sufficient drag to counterbalance the weight of any amount of ascending solids. The above two states actually correspond to fixed and moving beds, respectively, and both are homogeneous solutions. However, two-phase solutions also do not form if G_s is too low when U_g is greater than U_{mf}. Instead, homogeneous solutions form because force balance can be achieved, where stability criteria play no role and $N_{st} = N_T$. That is, Eq. (2.41) is essentially consistent with Eq. (2.40).

Therefore, by integrating Eqs. (2.21), (2.23), (2.25–2.27) and (2.34) concerned with mass and momentum conservation with the unified stability condition

Eq. (2.42) for all heterogeneous regimes in fluidization, the EMMS model can be summarized as follows:

$$\text{The EMMS model} \begin{cases} N_{\text{st}} = \min \text{ for all fluidization regimes} \\ F_{\text{i}}(X) = 0\,(i = 1, 2, \ldots, 6) \\ U_{\text{sc}} \geq 0,\ U_{\text{sf}} \geq 0,\ U_{\text{si}} \geq 0 \end{cases} . \tag{2.43}$$

2.3 Solution of the EMMS Model

From the above discussion and formulation, the general flow structure and regime transition in gas-solid fluidization systems can be predicted by solving the EMMS model, with outputs $\boldsymbol{X} = \{\varepsilon_{\text{f}}, \varepsilon_{\text{c}}, a_{\text{f}}, a_{\text{c}}, f, U_{\text{f}}, U_{\text{c}}, U_{\text{pf}}, U_{\text{pc}}, d_{\text{cl}}\}$ and various energy terms from the specified operating conditions and material properties. This constitutes a nonlinear non-equilibrium optimization problem with ten variables. As a result, it is nearly impossible to derive analytical solutions to the EMMS model. Even the solution of the original EMMS model that does not consider the acceleration of the dilute and dense phases required the use of general-purpose optimization software, such as the general reduced gradient (GRG) algorithm, in the early stage of this model (Li 1987; Li and Kwauk 1994). However, the GRG algorithm is inconvenient to use and suffers from divergence problems (Li et al. 1988b). Later, by using simplified stability conditions to determine the two variables ε_{f} and ε_{c} and reducing the cluster equation and drag coefficient (Xu and Li 1998), a basic analytical solution to the original EMMS model was obtained. Unfortunately, the result obtained deviated from the original solution. Li et al. (1999) then simplified the nonlinear optimization problem by solving a set of nonlinear equations, although a full analytical solution of the EMMS model is still impossible. More recently, Ge and Li (2002) explored the detailed characteristics of solutions and their theoretical implications by retrieving all missing roots using a rigorous numerical approach, which enabled the physical mapping of the fluidization regimes.

2.3.1 Analytical Solution of the Original EMMS Model

Although the original EMMS model cannot be directly applied in the TFM, this subsection still introduces an analytical solution to the original EMMS model to gain insight into its main mathematical characteristics (Cheng 2001). When $a_{\text{c}} = a_{\text{f}} = 0$, only eight structure parameters (ε_{f}, ε_{c}, f, U_{f}, U_{c}, U_{pf}, U_{pc}, and d_{cl}) remain in the EMMS model which can be solved by minimizing the energy consumption under constraints given by six nonlinear equations.

Li et al. (1999) proposed that the dilute phase is always at the critical state between heterogeneity and homogeneity, and the voidage of the dilute phase should be equal to the average voidage under the conditions of saturation carrying capacity at a specified gas velocity; that is,

$$\varepsilon_{\mathrm{f}} = \varepsilon_{\mathrm{uni}}\left[U_{\mathrm{g}}, G_{\mathrm{s}}^{*}\left(U_{\mathrm{g}}\right)\right]. \tag{2.44}$$

However, this value is not easy to determine because $G_{\mathrm{s}}^{*}(U_{\mathrm{g}})$ itself is calculated from the EMMS model, so global iterations are needed to determine ε_{f}, and the algorithm could be computationally expensive and unstable. For gas-solid systems, $N_{\mathrm{st}} = \min$ occurs at $\varepsilon_{\mathrm{f}} \to 1$ and $\varepsilon_{\mathrm{c}} \to \varepsilon_{\mathrm{mf}}$, whereas $W_{\mathrm{st}} = \min$ corresponds to a uniform structure with $\varepsilon_{\mathrm{f}} \to \varepsilon_{\mathrm{uni}}$ and $\varepsilon_{\mathrm{c}} \to \varepsilon_{\mathrm{mf}}$. For uniform suspensions, the gas-solid slip velocity is thought to be equal to the terminal velocity of the particles,

$$u_{\mathrm{s}} = \frac{U_{\mathrm{g}}}{\varepsilon_{\mathrm{uni}}} - \frac{U_{\mathrm{p}}}{1-\varepsilon_{\mathrm{uni}}} \approx u_{\mathrm{t}}. \tag{2.45}$$

Therefore, the voidage $\varepsilon_{\mathrm{uni}}$ for a uniform suspension can be approximated as

$$\varepsilon_{\mathrm{uni}} = \frac{U_{\mathrm{g}} + U_{\mathrm{p}} + u_{\mathrm{t}} - \sqrt{\left(U_{\mathrm{g}} + U_{\mathrm{p}} + u_{\mathrm{t}}\right)^{2} - 4u_{\mathrm{t}}U_{\mathrm{g}}}}{2u_{\mathrm{t}}}. \tag{2.46}$$

Using the values of ε_{f} and ε_{c} for a gas-solid system, the original EMMS model can simply be solved analytically to obtain the remaining six variables (f, U_{f}, U_{c}, U_{pf}, U_{pc}, and d_{cl}) from the sub-model consisting of six algebraic formulae. The details to derive the analytical solution follow below:

By rearranging Eq. (2.27),

$$U_{\mathrm{pc}} = \frac{U_{\mathrm{p}} - (1-f)U_{\mathrm{pf}}}{f}. \tag{2.47}$$

Substituting Eqs. (2.4, 2.5) and (2.47) into Eq. (2.26) gives

$$U_{\mathrm{pf}} = \frac{(1-\varepsilon_{\mathrm{f}})(1-\varepsilon_{\mathrm{c}})}{(\varepsilon_{\mathrm{f}}-\varepsilon_{\mathrm{c}})(1-f)}\left[U_{g} - \frac{\varepsilon_{\mathrm{c}}}{1-\varepsilon_{\mathrm{c}}}U_{\mathrm{p}} - (1-f)U_{\mathrm{sf}} - fU_{\mathrm{sc}}\right]. \tag{2.48}$$

Thus, we get

$$U_{\mathrm{c}} = U_{\mathrm{sc}} + \frac{\varepsilon_{\mathrm{c}}}{1-\varepsilon_{\mathrm{c}}}U_{\mathrm{pc}}, \tag{2.49}$$

$$U_{\mathrm{f}} = U_{\mathrm{sf}} + \frac{\varepsilon_{\mathrm{f}}}{1-\varepsilon_{\mathrm{f}}}U_{\mathrm{pf}}. \tag{2.50}$$

If $a_{\mathrm{c}} = a_{\mathrm{f}} = 0$, we can solve the force balance of (2.20), (2.22), and (2.24) to deduce:

$$m_{\mathrm{f}}F_{\mathrm{f}} = (1-\varepsilon_{\mathrm{f}})\left(\rho_{\mathrm{p}} - \rho_{\mathrm{g}}\right)g, \tag{2.51}$$

$$m_c F_c = (1-\varepsilon)\left(\rho_p - \rho_g\right)g, \tag{2.52}$$

$$m_i F_i = f(1-f)(\varepsilon_f - \varepsilon_c)\left(\rho_p - \rho_g\right)g, \tag{2.53}$$

where

$$1-\varepsilon = (1-\varepsilon_f) + f(\varepsilon_f - \varepsilon_c). \tag{2.54}$$

By expanding and rearranging Eqs. (2.51–2.53), we obtain three nonlinear equations for three independent variables (U_{sf}, U_{sc} and f) because the interface gas-solid slip velocity U_{si} can be determined from Eq. (2.6),

$$0.15\left(\frac{\rho_g d_p}{\mu_g}\right)^{0.687} U_{sf}^{1.687} + U_{sf} - \varepsilon_f^{4.7}\frac{(\rho_p - \rho_g)gd_p^2}{18\mu_g} = 0, \tag{2.55}$$

$$\begin{aligned} &0.15\left(\frac{\rho_g d_p}{\mu_g}\right)^{0.687} U_{sc}^{1.687} + U_{sc} \\ &-\frac{\varepsilon_c^{4.7}}{1-\varepsilon_c}\frac{(\rho_p - \rho_g)gd_p^2}{18\mu_g}[(1-\varepsilon_f) + (\varepsilon_f - \varepsilon_c)f] = 0 \end{aligned}, \tag{2.56}$$

$$0.15\left(\frac{\rho_g d_{cl}}{\mu_g}\right)^{0.687} U_{si}^{1.687} + U_{si} - (1-f)^{5.7}(\varepsilon_f - \varepsilon_c)\frac{(\rho_p - \rho_g)gd_{cl}^2}{18\mu_g} = 0. \tag{2.57}$$

Substituting Eqs. (2.51–2.54) into Eq. (2.16) leads to

$$N_{st} = \frac{\rho_p - \rho_g}{\rho_p} g\left\{U_g + \left(fU_c - U_g\right)\frac{(\varepsilon_f - \varepsilon_c)f^2}{1-\varepsilon_f + (\varepsilon_f - \varepsilon_c)f}\right\}. \tag{2.58}$$

Therefore, the analytical solution of the original EMMS model can be generally summarized as the set of Eqs. (2.34), (2.47–2.50), and (2.55–2.58).

2.3.2 Numerical Solution

In the TFM, mean voidage ε can be determined first. Thus, voidage (ε_f and ε_c) for the dilute and dense phases as well as the dense phase fraction (f) can be correlated by the following equation:

$$\varepsilon = f\varepsilon_c + (1-f)\varepsilon_f. \tag{2.59}$$

As in the original EMMS model, a system defined by ten variables (ε_f, ε_c, f, U_f, U_c, U_{pf}, U_{pc}, d_{cl}, a_c, and a_f) with seven constraints from dynamical equations including Eq. (2.59) should be closed by including the minimization constraint for energy consumption (N_{st}) in the updated EMMS model.

Because minimization of N_{st} is actually equivalent to a pair of well-defined ε_c and ε_f, the whole model can be solved by determining the minimum of N_{st} for all pairs ε_c and ε_f within a limited range. The unified stability condition in all heterogeneous fluidization regimes can be assumed to be $\varepsilon_c = \varepsilon_{mf}$ and $\varepsilon_f \to 1$, corresponding to $N_{st} \to$ min. However, the dilute phase should also contain particles ($\varepsilon_f < 1$) and weak heterogeneity should still exist even beyond choking. Therefore, the highest ε_f must be less than 1 so that heterogeneity can exist in real gas-solid systems. In theory, a rational value of ε_f should be determined from Eq. (2.44); however, this is impossible at present because certain global iterations are involved. Ge and Li (2002) found that ε_{max} indeed corresponds to this critical value, and it can be calculated directly from U_g and G_s for a specified gas-solid system. It should be noted that ε_{max} is not the lowest voidage at which homogeneity can exist, although it is the highest voidage where heterogeneity can. For most aggregative systems, ε_{max} is very close to unity and can be approximated as 0.9997 (Matsen 1982), but a particulate regime can exist at voidage near ε_{mf}. Ge and Li (2002) proposed that the upper limit of ε_f is ε_{max}, and the minimum of N_{st} can be determined by traversing ε_f and ε_c within the interval $[\varepsilon_{mf}, \varepsilon_{max}]$.

Wang and Li (2007) provided the following scheme to solve the ten variables in the updated EMMS model:

1. For a given system with specified U_g, G_s, ε, traverse ε_c and ε_f within interval $[\varepsilon_{mf}, \varepsilon_{max}]$;
2. Calculate volume fraction of dense phase f using Eq. (2.59);
3. Determine a_c and a_f within $[-g, a_{max}]$. Here a_{max} is a system-dependent value;
4. Calculate U_{sc} and U_{sf} using Eqs. (2.21), (2.23) and (2.25);
5. Use U_{sf} and U_{sc} to determine U_f, U_c, U_{pf} and U_{pc} from Eqs. (2.47–2.50);
6. Calculate d_{cl} using Eq. (2.34);
7. Calculate U_{si} from its definition and either Eqs. (2.21) or (2.25), denoting the difference as ΔU_{si};
8. Compare ΔU_{si} with the convergence criterion. If converged then store the value and continue traversing ε_c and ε_f within $[\varepsilon_{mf}, \varepsilon_{max}]$ until finish, otherwise return to step 3;
9. Find the optimal root through minimizing N_{st} among all possible roots satisfying convergence with respect to ΔU_{si}.

Unfortunately, the common approaches to solve nonlinear equations, such as the dichotomizing search, were not suitable for step 7 because a thorough study on the variation of ΔU_{si} with ε_c or ε_f was lacking. Although this scheme has achieved reasonable results, it fails to confirm the existence of multiple roots. Using this scheme, Ge and Li (2002) found that the solutions to the EMMS model can be classified into five types. With this in mind, the intervals without solutions can be excluded first, allowing the dichotomizing search to be applied to the remaining intervals with one and two solutions, speeding up the calculation greatly. Using this scheme, a complete and accurate solution to the EMMS model can be determined in less than one second by a mainstream CPU.

Based on the above scheme, an online program to numerically solve the original EMMS model without considering the acceleration of the two phases was developed and is available at http://emms.mpcs.cn/emmsmodel.php. Using this program, one can specify the material and operational parameters of a fluidized bed and determine its flow structure from the EMMS model. For instance, for a FCC/air system with $U_g = 2.1$ m/s and $G_s = 32$ kg/m^{2}s, results of $\varepsilon_f = 0.9997$, $\varepsilon_c = 0.5$ and $\varepsilon = 0.81034$ are obtained.

Traversing ε_f and ε_c within a limited range to find the minimum of N_{st} is a highly parallel computational process and could be implemented by graphics processing units (GPU). The 2D computational domain is initially partitioned into small steps by a CPU, and the cell information is then transferred to a corresponding GPU thread. Thus, the conservation equations can be solved in parallel to obtain all N_{st} in all cells, which are finally transferred back to the CPU to find the optimal solution to the EMMS model. Because of the powerful computational capacity of a GPU, the EMMS model can be solved at least two orders of magnitude faster than when using CPU.

With the determination of the ten parameters in the EMMS model, the so-called EMMS drag coefficient, accounting for the heterogeneous structure in gas-solid fluidization, can be derived to modify the hydrodynamic disparity between homogeneous and heterogeneous fluidization instead of using the value calculated by Wen and Yu (1966) based on homogeneous fluidization. The EMMS drag coefficient is determined by integration with the TFM through a user-defined function, and will be discussed in detail in Chap. 6.

2.3.3 Critical Conditions for Choking

Choking is an important phenomenon in fluidization engineering and appears at the boundary between fast fluidization and dilute pneumatic transport, at which heterogeneous structures are suddenly replaced by a uniform suspension or vice versa.

From the viewpoint of the EMMS theory (Li and Kwauk 1994), the choking point corresponds to the transition of the PFC to the FD regime, which needs to satisfy both $W_{st} = \min$ constrained by $\varepsilon_c = \varepsilon_{mf}$ in the PFC regime and $W_{st} = \min$ unconditionally in the FD regime. Figure. 2.9a shows the changes in W_{st} calculated with respect to $N_{st} = \min$ for the PFC regime and to $W_{st} = \min$ for the FD regime. The two curves cross each other at point B, which defines the critical conditions (Eq. (2.40)) at which the two-phase structure of dense fluidization separates into the uniform structure of dilute transport (Li et al. 1992); thus the cross-over at point B is taken as the criterion to determine the choking point. When $U_g < U_{pt}$, $(W_{st})_{PFC}$ is less than $(W_{st})_{FD}$; therefore, the dominant dynamics generates heterogeneous structure, and $N_{st} = \min$ results in a distinctive two-phase structure with $\varepsilon_c \to \varepsilon_{mf}$ and $\varepsilon_f \to 1$. When $U_g > U_{pt}$, $(W_{st})_{PFC}$ is greater than $(W_{st})_{FD}$, and the dominant dynamics generates homogeneous structure. Another alternative represented by $W_{st} = G_s g(\rho_p - \rho_f)/\rho_p$ for an ideal dilute homogeneous structure possesses even

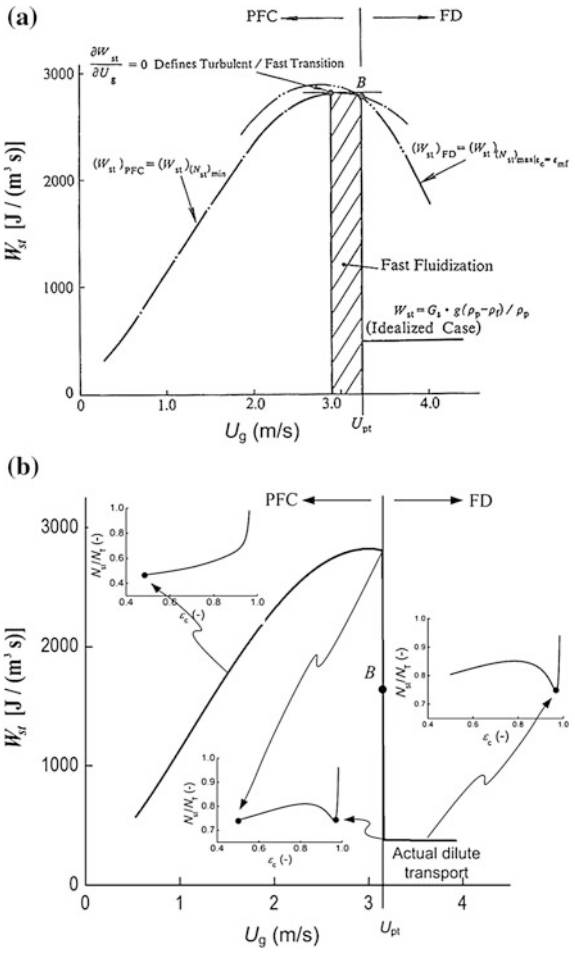

Fig. 2.9 Variation of W_{st} with gas velocity in FCC/air systems under different stability conditions: (**a**) $N_{st} = \min$ for the PFC regime and $W_{st} = \min$ for the FD regime; (**b**) $N_{st} = \min$ for all heterogeneous fluidization regimes (Li and Kwauk 1994)

lower values of W_{st}, and is therefore more representative of the preferred dominant dynamics. Despite its agreement with experimental phenomena, the above results are imperfect in two aspects; i.e., the dilute phase should also contain particles ($\varepsilon_f < 1$) below choking, and weak heterogeneity should still exist beyond choking. Therefore, a real fluidization state can be imagined between the two above-mentioned modes because gas-solid systems are not in the ideal dilute transport regime.

As stated above, Ge and Li (2002) proposed that ε_f at the beginning of clustering is equal to ε_{max}, and verified that the EMMS model is capable of describing this hydrodynamic effect. However, the kinetics of particle suspensions were not incorporated, which led to the prediction $\varepsilon_f = 1$. By thorough study of the numerical solution to the EMMS model, Ge and Li (2002) proposed Eq. (2.41) in place of Eq. (2.40) as the criterion for choking. Thus, the remaining heterogeneity observed beyond choking can be explained, and choking can be interpreted as the shift between two stable states.

Figure 2.9b illustrates the choking point B defined by the unified stability condition $N_{st} = \min$ under the same operating conditions as in Fig. 2.9a. It is clear that the predictions of the two methods agree well with each other. When $U_g < U_{pt}$, $N_{st} = \min$ results in only one heterogeneous structure represented by $\varepsilon_c = \varepsilon_{mf}$ and $\varepsilon_f = \varepsilon_{max}$, corresponding to the PFC regime defined by $(W_{st})_{(N_{st})_{min}} = \min$. When $U_g = U_{pt}$, $N_{st} = \min$ gives rise to the coexistence of two heterogeneous states represented by $\varepsilon_c = \varepsilon_{mf}$ and $\varepsilon_c = \varepsilon_o$ at the same $\varepsilon_f = \varepsilon_{max}$, corresponding to the critical state defined by Eq. (2.40). When $U_g > U_{pt}$, $N_{st} = \min$ leads to just one heterogeneous structure again, which is represented by $\varepsilon_c = \varepsilon_o$ and $\varepsilon_f = \varepsilon_{max}$, corresponding to the FD regime defined by $(W_{st})_{(N_{st})_{max}}\big|_{\varepsilon=\varepsilon_{mf}} = \min$. Obviously, the unified stability condition $N_{st} = \min$ not only simplifies the calculation process, but also enables the complete description of real fluidization states at all fluidization gas velocities.

2.3.4 Regime and Operation Diagram for Gas-Solid Systems

For any gas-solid system, a series of regime transitions occur and three essential regimes of operation can prevail in succession with increasing gas velocity: PD, PFC and FD. The EMMS model provides quantitative criteria for the transitions between fluidization regimes as well as being a tool to determine the fluidization regime given operating conditions and material properties. It is generally accepted that the minimum fluidization velocity U_{mf} corresponds to the transition between PD and PFC regimes; that is, the transition from fixed to fluidized beds. As discussed above, N_{st} characterizes the stability of a gas-solid system and governs the transition between PFC and FD regimes at U_{pt}, as stipulated in Eqs. (2.40) and (2.41).

Wang et al. (2008) obtained an intrinsic diagram for an air-FCC system ($d_p = 54$ μm, $\rho_p = 930$ kg/m^3) using the original EMMS model. As shown in Fig. 2.10, the saddle area marked by the dashed line implies the coexistence of the dense and dilute flow regions with $G_s = K^*$, in which the G_s curves feature a constant segment corresponding to the transition between the PFC and FD regimes. The area indicated by PFC on the right is the dense flow region with $G_s > K^*$, whereas that marked FD on the left is the dilute flow region with $G_s < K^*$. Point D is the critical point for the coexistence of the dense and dilute flow regions. If U_g is larger than the gas velocity corresponding to this point, the system enters the dilute flow region. Alternatively, if G_s is larger than the solid flow rate corresponding to this point, the system falls into the dense flow region. Choking arises as a boundary between dilute transport and dense upflow, above which the flow transition is an abrupt change. In contrast, the non-choking transition above the critical point is a smooth and continuous transition between dilute transport and dense upflow. It should be noted that this intrinsic map of the fluidization regimes does not include the effects of the reactor geometry and size

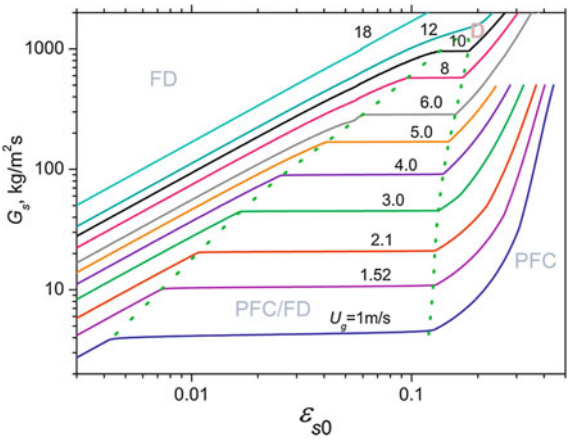

Fig. 2.10 Dependence of regime transitions on gas velocity in gas-solid two-phase flow (ε_{s0} is the average solid concentration over the whole vessel) (Wang et al. 2008). Reproduced from ref. Wang et al. (2008) by permission of John Wiley & Sons Ltds

because the original EMMS model allows the global and steady state performance of fluidization systems to be described.

The transitions within the PFC regime, bubbling/turbulent and turbulent/fast, can be distinguished by the energy term W_{st}. As illustrated in Fig. 2.11, the first transition takes place at

$$\partial W_{st}/\partial G_s = 0, \tag{2.60}$$

which corresponds to a common dense phase fraction of $f = 0.5$ regardless of gas velocity and solid flow rate. At this point, it is difficult to identify which phase is continuous; that is, a phase inversion from continuous dense phase to continuous dilute phase is taking place, so the system can be considered to have reached a state of maximum heterogeneity. This inversion can be construed to mark the transition from bubbling to turbulent fluidization. As indicated in Fig. 2.9a, the regime transition between turbulent and fast fluidization can be mathematically defined as

$$\partial W_{st}/\partial U_g = 0, \tag{2.61}$$

corresponding to the maximal W_{st} with respect to gas velocity. However, this transition is difficult to observe in practice, even though it is often included in the overall designation of high-velocity fluidization and CFBs (Reh 1971).

A typical gas-solid two-phase flow system, such as a CFB, is characterized not only by local heterogeneous flow structure but also by an overall non-uniform distribution for bed density. For example, Li and Kwauk (1980) noted that in fast fluidization, a dilute region at the top coexists with a dense region at the bottom, and claimed this axial profile possessed an "S" shape. Li and Kwauk (1994) also pointed out that at any constant gas velocity, S-shaped profiles can exist only within certain limits of the solid inventory, and a small bed height corresponding to a short horizontal section in Fig. 2.10 would hinder the development of an

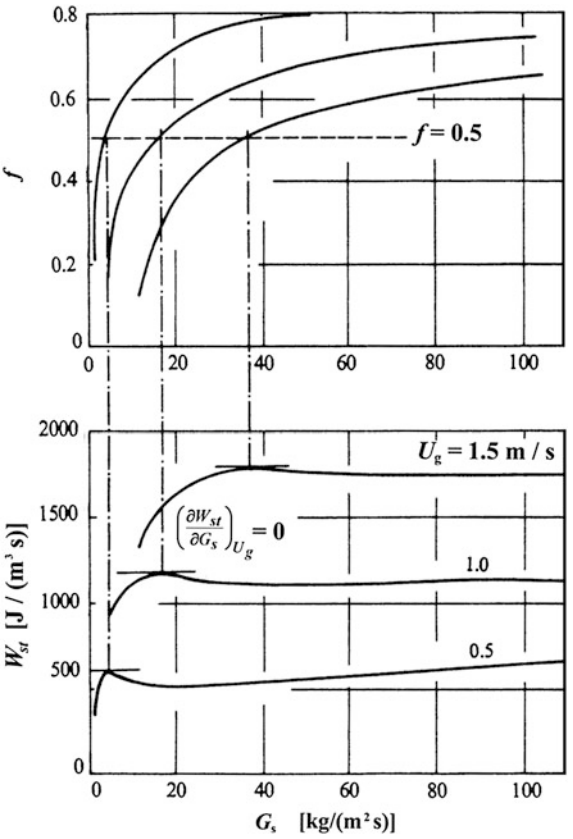

Fig. 2.11 Transition from bubbling to turbulent fluidization in an air-FCC system (Li and Kwauk 1994)

S-shaped profile. Therefore, to realize a given regime, certain global conditions need to be satisfied in addition to intrinsic fluid dynamics.

2.4 The EMMS Drag for CFD

Drag calculations in heterogeneous gas-solid systems are a challenge for CFD simulations because of the complexity of gas-solid flow resulting from the highly nonlinear and multiscale nature of drag terms (Yang et al. 2003; Wang and Li 2007). Although many correlations based on the assumption of homogeneous suspensions have been proposed to quantify drag, both uncertainties and discrepancies still remain because dynamic multiscale heterogeneity is one of the inherent characteristics of gas-solid fluidization systems. Resolving a gas-solid fluidization system into a gas-rich dilute phase and a solid-rich dense phase, the EMMS model characterizes the multiscale structures of a gas-solid system using eight structural parameters, making it possible to quantify the multiscale gas-solid interactions in a fluidization system.

2.4.1 Deficiencies of Traditional Drag Models

Drag arises from the relative motion of particles and fluid and is defined as

$$F = \frac{1}{2}\rho_f C_D A U_s^2, \tag{2.62}$$

where C_D, A, and U_s are the drag coefficient, projected area of a particle in the plane perpendicular to the flow direction, and particle-fluid slip velocity, respectively.

For a single particle in an infinite flow field in the absence of other particles, the drag coefficient can be expressed as a function of Reynolds number *Re* (Flemmer and Banks 1986),

$$C_D = C_{D0} = \begin{cases} 24/\mathrm{Re} & \text{for } \mathrm{Re} < 0.2 \\ 24/\mathrm{Re} + 3.6/\mathrm{Re}^{0.313} & \text{for } \mathrm{Re} < 1000 \\ 0.44 & \text{for } \mathrm{Re} < 3 \times 10^5 \end{cases}. \tag{2.63}$$

This drag coefficient is also called the standard drag coefficient C_{D0}. There are numerous correlations for the standard drag coefficient reported in the literature, which have been summarized comprehensively (Perry and Green 2007).

For a particle in a homogeneous suspension, the surrounding particles may either hinder or accelerate its motion, leading to an effective drag coefficient C_D that differs from the standard drag coefficient C_{D0}. Numerous correlations to relate these two drag coefficients have been published, among which the Wen-Yu correlation (Wen and Yu 1966) is best known,

$$C_D = C_{D0}\varepsilon^{-4.7}. \tag{2.64}$$

Note that the superficial slip velocity based on local voidage should be used in the above correlation,

$$U_s = U_g - U_p\varepsilon/(1-\varepsilon). \tag{2.65}$$

Many gas-solid systems exhibit significant local and overall heterogeneity instead of forming typical homogeneous suspensions. This structural heterogeneity mainly resulting from particle aggregation significantly influences the effective drag coefficient. As observed in Fig. 2.12, $\bar{C}_D$ varies significantly with different structures in a given volume with $\varepsilon_a = \varepsilon_b = \varepsilon_c$ for a gas-solid system. The formation of local structure leads to a decrease in $\bar{C}_D$ from (a) to (b), even though the average parameters for these two structures are identical. A core-annulus distribution of local structure leads to a further decrease of $\bar{C}_D$ from (b) to (c), indicating that the formation of non-uniform distribution reduces the global transfer rate. This demonstrates that $\bar{C}_D$ is not only a function of *Re* and local voidage, but also depends on the formation of heterogeneous structures. Therefore, correlating the drag coefficient to average parameters such as mean slip velocity must lead to

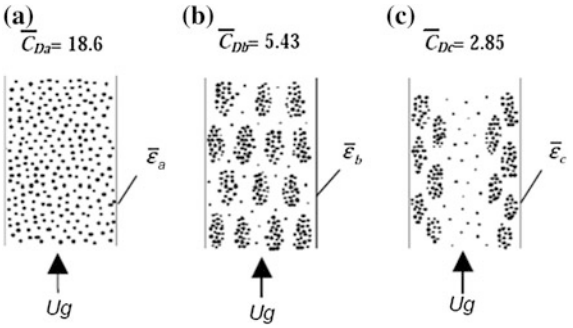

Fig. 2.12 Effect of structural heterogeneity on the effective drag coefficient C_D in a given volume with the same amount of particles and gas flow rate (Li and Kwauk 2001)

large discrepancies in the transfer rate. As a result, average parameters are not sufficient for theoretical and engineering calculations.

Although different approaches have been developed to characterize transport properties in non-homogeneous gas-solid systems (Helland et al. 2000; Zhang and Vanderheyden 2002), the EMMS-based drag model provides a relatively accurate formulation of drag coefficient by taking into account the effects of heterogeneous structures (Yang et al. 2003; Wang and Li 2007).

2.4.2 EMMS Drag

In the original EMMS model, the dilute and dense phases are described by gas and solid velocities (U_f, U_c, U_{pf}, and U_{pc}) and voidage in each phase (ε_f and ε_c), whereas the structural heterogeneity is characterized by cluster diameter (d_{cl}) and dense phase fraction (f). With these parameters calculated from the model, the multiscale gas-solid interactions in gas-solid flow can be quantitatively characterized by analyzing the superficial drag coefficient C_{Dc} for a single particle or cluster in the system.

For the dense phase, C_{Dc} for a single particle can be expressed as

$$C_{Dc} = F_c \Big/ \left(\frac{\pi d_p^2}{4} \frac{\rho_g U_{sc}^2}{2} \right) = \frac{8(1-\varepsilon)(\rho_p - \rho_g)g}{m_c \pi d_p^2 \rho_g \left(U_c - \dfrac{U_{pc}\varepsilon_c}{1-\varepsilon_c} \right)^2}. \tag{2.66}$$

Similarly, for the dilute phase

$$C_{Df} = F_f \Big/ \left(\frac{\pi d_p^2}{4} \frac{\rho_g U_{sf}^2}{2} \right) = \frac{8(1-\varepsilon_f)(\rho_p - \rho_g)g}{m_f \pi d_p^2 \rho_g \left(U_f - \dfrac{U_{pf}\varepsilon_f}{1-\varepsilon_f} \right)^2}. \tag{2.67}$$

For the interaction between the two phases, the superficial drag coefficient C_{Di} for a single cluster is

$$C_{\mathrm{Di}} = F_{\mathrm{i}} \Big/ \left(\frac{\pi d_{\mathrm{cl}}^2}{4} \frac{\rho_{\mathrm{g}} U_{\mathrm{si}}^2}{2} \right) = \frac{8f(\varepsilon - \varepsilon_{\mathrm{c}})(\rho_{\mathrm{p}} - \rho_{\mathrm{g}})g}{m_{\mathrm{i}} \pi d_{\mathrm{cl}}^2 \rho_{\mathrm{g}} \left(U_{\mathrm{f}} - \frac{U_{\mathrm{pc}} \varepsilon_{\mathrm{f}}}{1 - \varepsilon_{\mathrm{c}}} \right)^2 (1 - f)^2}, \tag{2.68}$$

where m_{c}, m_{f}, and m_{i} are the particle or cluster number in a unit bed volume.

Li et al. (1993) quantitatively compared these three drag coefficients by solving the original EMMS model. To characterize the average gas-solid interaction in the system, they defined an average drag coefficient as follows:

$$\bar{C}_{\mathrm{D}} = \frac{4 d_{\mathrm{p}} \rho_{\mathrm{p}} g}{3 \rho_{\mathrm{g}} \left(U_{\mathrm{g}} - \frac{G_{\mathrm{s}} \varepsilon}{\rho_{\mathrm{p}} (1 - \varepsilon)} \right)^2}, \tag{2.69}$$

where the average voidage ε, gas velocity U_{g}, and solid circulation rate G_{s} can be correlated with the preceding structural parameters using Eqs. (2.54), (2.26), and (2.27), respectively. Although the average drag coefficient for the whole system differed from that for the cell in a CFD simulation, both reflected characteristics derived from averaging methods for drag calculations, albeit to different extents.

As revealed in Fig. 2.13, a significant difference exists between the dense and dilute phases not only for gas-solid slip velocity U_{sc} but also for superficial drag coefficient C_{Dc}. All C_{Dc} are high because of the low U_{sc} at minimum fluidization. C_{Dc} becomes even higher with increasing U_{g} because of decreasing U_{sc}. However, the interfacial gas-solid slip velocity U_{si} is much higher than U_{sc}, and increases with increasing U_{g}, leading to low interfacial superficial drag coefficient C_{Di}. For a single particle, both U_{sc} and C_{Dc} are constant in the dilute phase in the fluidization regime, but exhibit abrupt changes at U_{pt} corresponding to choking, and then gradually approach U_{t} and C_{Dc}, respectively, with increasing U_{g}. The average drag coefficient and U_{sc} change differently compared to all other phase-related terms, and therefore are not sufficient to fully characterize gas-solid interactions in a system. The average drag coefficient reaches quite low values (less than 0.1) at high gas velocity, which is not reasonable.

The volumetric drag coefficient β, which is the drag acting on all particles in a simulated cell divided by the average gas-solid slip velocity, is usually used in the type A TFM (Gidaspow 1994),

$$\beta = \frac{\varepsilon^2}{U_{\mathrm{s}}} \sum F. \tag{2.70}$$

If the heterogeneous structures in the cell are not considered, β can be readily derived from the Wen-Yu correlation, which is generally set equal to the standard volumetric drag coefficient β_0,

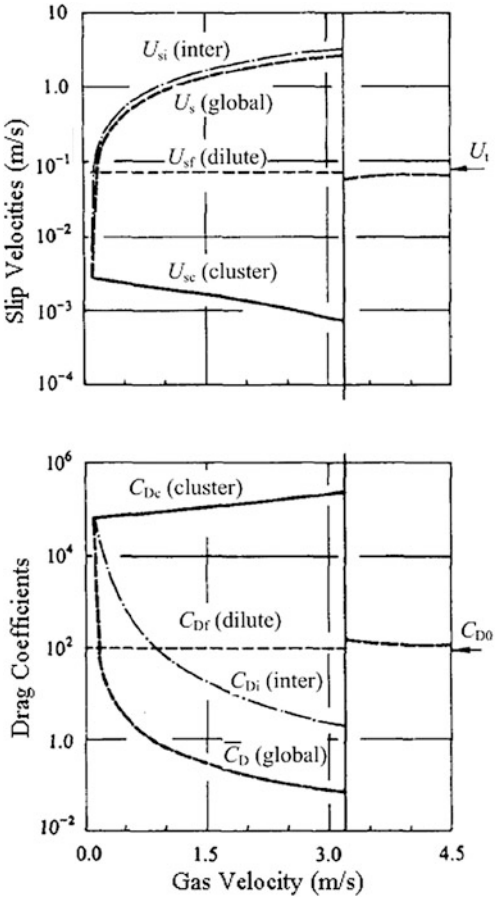

Fig. 2.13 Dependencies of slip velocities and drag coefficients on gas velocity in different phases for a FCC/air system ($d_p = 54$ mm, $\rho_p = 930$ kg/m^3, $G_s = 50$ kg/m^{2}s) (Li and Kwauk 1994)

$$\beta = \beta_0 = \frac{3}{4}\frac{\varepsilon(1-\varepsilon)}{d_p}\rho_g C_{D0}|u_s|\varepsilon^{-2.7}. \tag{2.71}$$

Correspondingly, the so-called EMMS-based volumetric drag coefficient can be expressed as follows:

$$\begin{aligned}\beta &= \frac{\varepsilon^2}{U_s}[fm_c F_c + m_i F_i + (1-f)m_f F_f] \\ &= \frac{\varepsilon^2}{U_s} f(\rho_p - \rho_g)(1-\varepsilon_c)(a_c + g)\end{aligned}. \tag{2.72}$$

Zhang et al. (2008) found that local voidage and *Re* are the two main factors affecting the EMMS-based volumetric drag coefficient β. Compared with β_0 calculated from the Wen-Yu correlation, β is clearly smaller because of the formation of heterogeneous structures. Higher *Re* results in a greater difference between

these two volumetric drag coefficients. To aid inclusion of the EMMS-based drag coefficient into the TFM without enormous computational cost, Yang et al. (2003) determined a correction factor for the drag coefficient with voidage according to the calculated results for a whole bed and in CFD simulations directly applied the calculated correction factor to each local cell. Wang and Li (2007) extended the EMMS model to the grid level of CFD simulations by producing a large matrix of drag coefficients that depended on global information to determine the structure-dependent drag coefficient for any cell in a CFD simulation through direct interpolation inside the matrix. The details of this process are presented in Chap. 6.

2.5 The Overall EMMS Model

The EMMS model describes local fluid dynamics of gas-solid systems, which depend on operating conditions and material properties. The overall fluid dynamics of gas-solid systems such as CFBs is much more significant to engineering, which deals with its space-dependent characteristics subject to boundary conditions. For axisymmetric equipment generally employed in engineering, the overall fluid dynamics can be resolved into radial and axial directions: core and wall regions for the former, and top and bottom regions for the latter.

2.5.1 Radial EMMS Model

Radial heterogeneity, generally referring to a dilute core region surrounded by a dense annular region next to the wall, is also related to $N_{st} = \min$ (Li 1987). According to the EMMS model, the local fluid dynamics of fluidized beds can be described by the eight parameters defined by Eq. (2.43). Because of radial heterogeneity in CFBs, the radial EMMS model can be expressed in a similar functional form to describe the fluid dynamics at a specified axial position and any radial position r:

$$\begin{cases} N_{st}(r) = \min \\ F_i(X)(r) = 0\,(i = 1, 2, \ldots, 6) \\ U_{sc}(r) \geq 0,\ U_{sf}(r) \geq 0,\ U_{si}(r) \geq 0 \end{cases}, \tag{2.73}$$

where $F_i(X)(r)$ denotes the mass and momentum conservation equations at r. Using these equations, it is possible to calculate all other local parameters from the profiles of gas velocity $U_g(r)$ and particle velocity $U_p(r)$. Unfortunately, only the average superficial gas velocity U_g and average superficial particle velocity U_p can be determined from experimental data. Therefore, $U_g(r)$ and $U_p(r)$ should be correlated with U_g and U_p as well as boundary conditions,

$$U_g = \frac{2}{R^2}\int_0^R U_g(r) r dr, \tag{2.74}$$

$$U_p = \frac{G_s}{\rho_p} = \frac{2}{R^2}\int_0^R U_p(r) r dr. \tag{2.75}$$

Besides the strong influence of the wall on the flow field, minimization of energy is considered the main governing factor that defines heterogeneity in the radial direction. For the total cross-section, a stable radial profile requires minimization of the cross-sectional average energy consumption to suspend and transport particles,

$$\bar{N}_{st}(r) = \frac{2}{R^2(1-\bar{\varepsilon})}\int_0^R N_{st}(r)[1-\varepsilon(r)] r dr = \min, \tag{2.76}$$

where the cross-sectional average bed voidage is defined as

$$\bar{\varepsilon}(r) = \frac{2}{R^2}\int_0^R \varepsilon(r) r dr. \tag{2.77}$$

Therefore, to fulfill both local and overall stability, all parameters adjust themselves radially in such a way that not only $N_{st}(r)$ at any radial position, but also $\bar{N}_{st}(r)$ for the whole cross-section is minimized in addition to the constraints of force balance, continuity and boundary conditions, yielding a radial profile governed by Eqs. (2.73)–(2.76) (Li 1987; Li et al. 1990).

In theory, it is possible to calculate the radial profiles of all parameters with the radial EMMS model from the specified operating conditions. However, the solution of the radial EMMS model involves a twofold optimization problem and is very sensitive to boundary conditions, so it is advisable to use as much experimental data as possible to simplify it further. Of the three important radial profiles for $U_g(r)$, $U_p(r)$ and $\varepsilon(r)$, at least one can be deduced from the other two using the proposed model. If radial heterogeneity is assumed to be distributed in terms of a heterogeneity factor $K(r)$, which is defined as the ratio of the equivalent cluster diameter to the particle diameter,

$$K(r) = \frac{d_{cl}(r)}{d_p}, \tag{2.78}$$

then $K(r)$ can be expressed as $K(\varepsilon(r))$ if the radial voidage profile $\varepsilon(r)$ is known; it should fulfill the boundary conditions: $K(\varepsilon_{mf}) = D_t/d_p$ and $K(1.0) = 1.0$. Now, the problem reduces to finding $K(r)$ satisfying energy minimization, force balance, continuity, and the given boundary conditions.

The radial profiles of parameters affecting the solid velocity $U_d(r)$ were calculated with the above simplified radial EMMS model (Li et al. 1990) using $\varepsilon(r)$ and gas throughput provided by Bader et al. (1988); these are presented in Fig. 2.14. $K(r)$ is small in the dilute core region, but increases dramatically near the wall

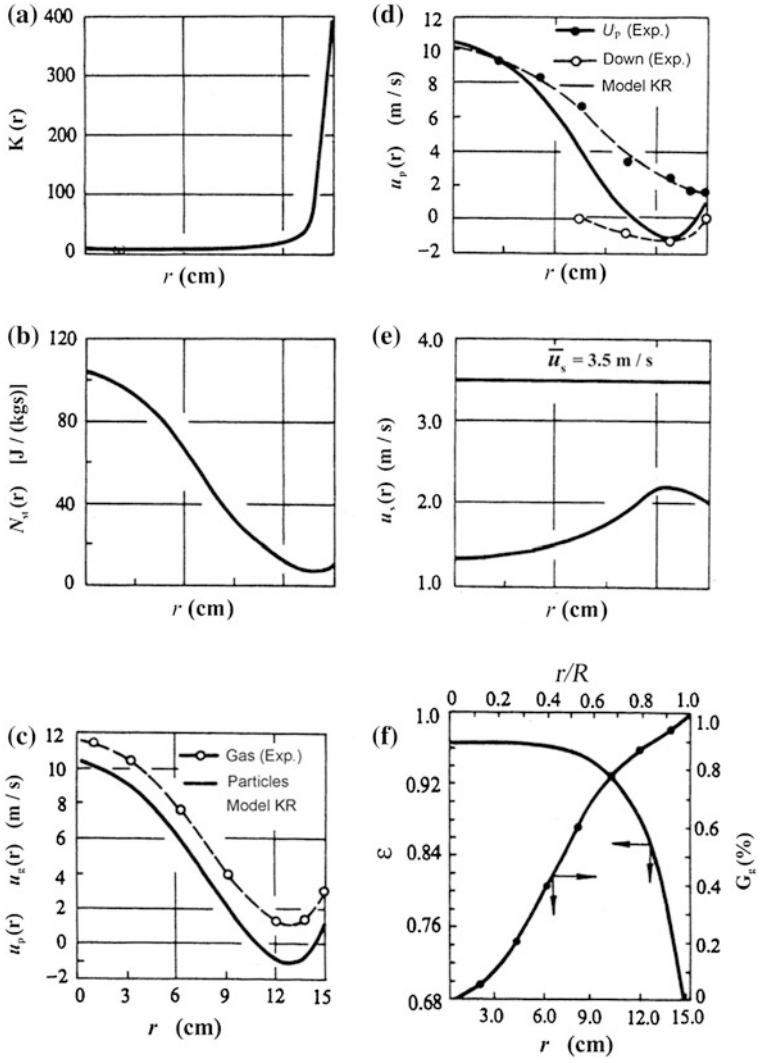

Fig. 2.14 Radial profiles (*solid lines*) of key parameters obtained from the radial EMMS model. Experimental results (*dashed lines*) are plotted for comparison (Li et al. 1990)

(Fig. 2.14a), indicating a nearly homogeneous structure in the core region, but a much more aggregated bed structure near the wall region. $N_{st}(r)$ is very high in the dilute core region and extremely low in the dense wall region (Fig. 2.14b), which leads to minimization of $\bar{N}_{st}$, and hence to a stable radial profile. As illustrated in Fig. 2.14c, the particle velocity calculated from the radial EMMS model approaches the experimental gas velocity deduced from Fig. 2.14f in the dilute core region, but decreases to a negative value in the dense wall region. Calculated and measured particle velocity profiles are compared in Fig. 2.14d, and show

reasonable agreement. The calculated radial profile of gas-solid slip velocity is presented in Fig. 2.14e. The lowest slip velocity occurs in the bed center because of the uniform structure in this region, while the highest is observed not far from the wall. The local slip velocity at any radial position is lower than the cross-sectional average slip velocity, implying that the high average slip velocity for the overall CFB reactor should be attributed not only to overall heterogeneity, but also to local heterogeneity resulting from the aggregation of particles.

2.5.2 Axial EMMS Model

Axial heterogeneity mainly refers to the coexistence of two different regions in terms of local fluid dynamics: a bottom dense region and a top dilute region. By considering the influence of particle acceleration on the axial heterogeneity of gas-solid fluidization systems, Cheng (2007) attempted to establish the so-called axial EMMS model.

Neglecting the radial heterogeneity at a given axial location, the axial EMMS model can also be expressed in a similar functional form to Eq. (2.43):

$$\begin{cases} N_{\mathrm{st}}(z) = \min \\ F_{\mathrm{i}}(X)(z) = 0\,(i = 1, 2, \ldots, 6) \\ U_{\mathrm{sc}}(z) \geq 0,\ U_{\mathrm{sf}}(z) \geq 0,\ U_{\mathrm{si}}(z) \geq 0 \end{cases}, \tag{2.79}$$

where $N_{\mathrm{st}}(z) = \min$ is equivalent to $\bar{N}_{\mathrm{st}}(r) = \min$ in Sect. 2.5.1, and $F_{\mathrm{i}}(X)(z)$ denotes the mass and momentum conservation equations at axial location z. The acceleration of the dilute phase a_{f} is assumed to be zero, whereas the acceleration of the dense phase a_{c} is defined as

$$a_{\mathrm{c}} = \frac{d\left(\dfrac{U_{\mathrm{pc}}}{1-\varepsilon_{\mathrm{c}}}\right)}{dt} = \frac{U_{\mathrm{pc}}}{1-\varepsilon_{\mathrm{c}}} \frac{\partial\left(\dfrac{U_{\mathrm{pc}}}{1-\varepsilon_{\mathrm{c}}}\right)}{\partial z}. \tag{2.80}$$

Equation (2.80) correlates the structural parameters at different axial locations, indicating the axial EMMS model enables the axial variation of heterogeneous structural parameters resulting from particle acceleration to be described.

Besides the local stability condition $N_{\mathrm{st}}(z) = \min$, a stable axial profile in CFBs also requires a global stability condition to define heterogeneity in the axial direction; that is, minimization of the average energy consumption to suspend and transport particles in the whole vessel,

$$\bar{N}_{\mathrm{st}}(z) = \frac{\int_0^{H_{\mathrm{t}}} [1-\varepsilon(z)] N_{\mathrm{st}}(z) dz}{\int_0^{H_{\mathrm{t}}} [1-\varepsilon(z)] dz} = \min, \tag{2.81}$$

where the average bed voidage at some axial location is defined as

$$\bar{\varepsilon}(z) = \varepsilon_c(z)f(z) + \varepsilon_f(z)[1 - f(z)]. \tag{2.82}$$

Therefore, the axial EMMS model can be summarized by Eqs. (2.79)–(2.81) assuming that $a_f = 0$ at any axial location. That is, all structural parameters would adjust themselves axially in such a way that not only $N_{st}(z)$ at any axial location, but also $\bar{N}_{st}(z)$ for the whole vessel is minimized in addition to the constraints of force balance, continuity and boundary conditions. From a mathematical point of view, the axial EMMS model is in essence a variational optimization problem, which is impossible to solve accurately at present because of computational limitations. Therefore, we tried to find a simplified solution to the axial EMMS model.

Li and Kwauk (1980) found that axial heterogeneity in fast fluidized beds is mainly characterized by a bottom dense region with average voidage ε_a and a top dilute region with average voidage ε^* that are bridged by a transition region to form an S-shaped profile:

$$\frac{\varepsilon - \varepsilon_a}{\varepsilon^* - \varepsilon} = \exp[-(z - Z_i)/Z_0], \tag{2.83}$$

where Z_i is the inflection in the profile and Z_0 is the characteristic length, which is the length of the transition section and can be correlated with ε_a and ε^* as follows,

$$Z_0 = 500\exp[-69(\varepsilon^* - \varepsilon_a)]. \tag{2.84}$$

Because $N_{st} = \min$ can be adopted as the unified stability condition for both the PFC and FD regimes, the EMMS model defined by Eq. (2.43) can be directly solved given U_g and G_s. No root implies the desired dynamics cannot be realized under the given operating conditions; one root indicates the gas-solid system operates in either the PFC or the FD regime; and two roots signify a two-regional axial voidage profile for the gas-solid system. For two roots, the parameters ε_a and ε^* can be respectively determined as follows:

$$\varepsilon_a = f\varepsilon_{ca} + (1 - f)\varepsilon_{fa}, \tag{2.85}$$

$$\varepsilon^* = f\varepsilon_c^* + (1 - f)\varepsilon_f^*. \tag{2.86}$$

Using the values of ε_a and ε^* thus calculated, and ΔP_{imp} computed from the solids inventory and geometry of the equipment, the height of the inflection point Z_i can be deduced from the pressure balance,

$$Z_i = \frac{\Delta P_{imp} - (1 - \varepsilon_a)\rho_p g H}{(\varepsilon_a - \varepsilon^*)\rho_p g}. \tag{2.87}$$

Equations (2.43) and (2.83)–(2.87) in fact constitute an empirical axial EMMS model, which can be used to predict axial heterogeneous profiles until it is possible to numerically solve the axial EMMS model of Cheng (2007).

Based on the above empirical axial EMMS model and the integration of parallel GPU and OpenMP algorithms, Liu et al. (2011) further developed a computational method to rapidly predict the full-loop hydrodynamics of complex gas-solid fluidization systems, which typically has segments with varying geometries and sizes. As presented in Fig. 2.15, the complex fluidization system is first separated into several simple segments with constant geometries and sizes. Corresponding to the total gas and solid flow rate of the system, each segment has different gas velocities and solid fluxes. The so-called section computing method is then used to apply the EMMS model in each segment. Each straight tube requires a single iteration of the EMMS model, whereas in each reducer multiple iterations are needed to determine the conditions necessary to generate the steady state under the specified gas velocity and solid flux. If the straight tube section operates near the choking point with two coexisting stable states, the axial EMMS model establishes an S-shaped axial voidage profile, whereas the radial voidage distribution is determined by relevant empirical correlations based on the predicted axial voidage profile. The global flow distribution is affected by both the pressure and solid mass balance in the whole fluidization system. A typical example of the application of this computational method can be found in Chap. 7.

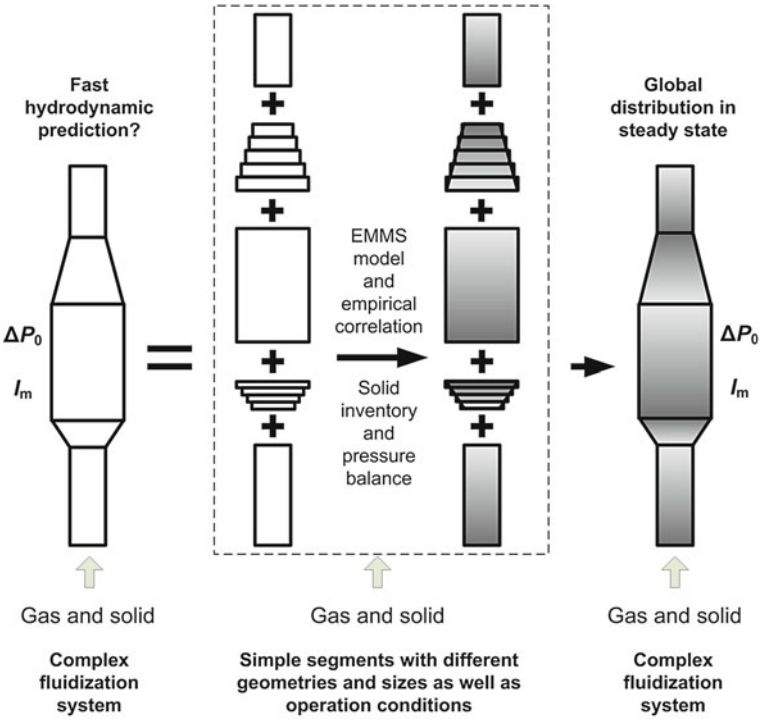

Fig. 2.15 Schematic of the principle behind the algorithm for rapid prediction of the global hydrodynamics of complex gas-solid fluidization systems

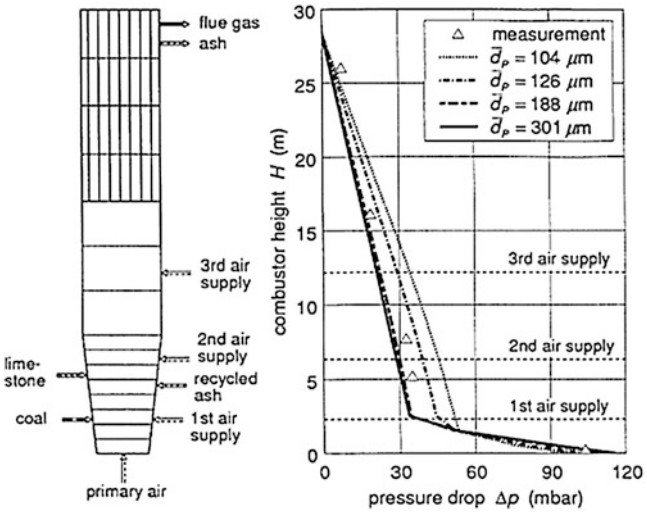

Fig. 2.16 Measured and calculated axial voidage profiles for different particle diameters (I_m = 16,600 kg, $\rho_p = 2700$ kg/m^3, $\rho_g = 0.32$ kg/m^3, $\mu_g = 4.485 \times 10^{-5}$ kg/(m s), $\varepsilon_{mf} = 0.46$) (Li et al. 1999). Reprinted from ref. Li et al. (1999), Copyright 2012, with permission from Elsevier

The axial EMMS model has also been used to simulate the WSK1 boiler at Bayer AG, Leverkusen, Germany, which is an industrial boiler with an atmospheric CFB combustion system. The total air supply is separated into three streams along the combustor height, yielding an increase in the superficial gas velocity from 4.0 to 6.0 m/s. The mean diameter of the bed material or ash was reasonably predicted by Li et al. (1996) to account for its dependence on both the size distribution and flow conditions. Figure 2.16 illustrates the calculated axial pressure profiles for different mean particle diameters, indicating good agreement with the measured data. It is evident that a smaller particle diameter results in a decrease in bed height, and an increase in solids transport and combustor height. Using the calculated mean particle diameter as a parameter in the model, the calculated solids elutriation is about 410 kg/s, which is consistent with measured values of 400–450 kg/s.

2.6 Problems to be Solved

Since the EMMS model was first proposed at the second International Conference on CFB Technology in 1988 (Li et al. 1988b), the model received both interest and criticism until it was verified in 2004 (Zhang et al. 2005). The EMMS model predicts the coexistence of dilute and dense phases as well as choking in gas-solid fluidization systems, and has been successfully integrated with the TFM to

simulate gas-solid systems giving results that agree with experimental data, providing proof of its rationality. However, the cluster diameter defined by Eq. (2.34) depends sensitively on the so-called maximal voidage ε_{max}, which may lead to unstable solutions generated by the EMMS model. Although the EMMS group has made many attempts to quantify particle clustering behavior (Liu et al. 2005; Liu et al. 2006), problems related to cluster diameter still persist and further effort is needed to solve them.

References

Bader R, Findlay J, Knowlton TM (1988) Gas/solid flow patterns in a 30.5 cm diameter circulating fluidized bed. In: Basu P, Large JF (eds) Circulating fluidized bed (CFB), vol 2. Pergamon Press, New York, pp 123–137

Chavan VV (1984) Physical principles in suspension and emulsion processing. In: Mujumdar AS, Mashelkar RA (eds) Advances in transport peocesses. Wiley, New York, pp 1–6

Cheng CJ (2007) Multi-scale modeling of the axial heterogeneous structure in circulating fluidized beds. Ph.D, Institute of Process Engineering, Chinese Academy of Sciences

Cheng CL (2001) Energy minimization multi-scale core-annulus model for CFBs. Ph.D, Institute Process of Engineering, Chinese Academy of Sciences

Cui H, Li J, Kwauk M, An H, Chen M, Ma Z, Wu G (2000) Dynamic behaviors of heterogeneous flow structure in gas-solid fluidization. Powder Technol 112(1–2):7–23

Flemmer RLC, Banks CL (1986) On the drag coefficient of a sphere. Powder Technol 48:217–221

Ge W, Chen F, Gao J, Gao S, Huang J, Liu X, Ren Y, Sun Q, Wang L, Wang W, Yang N, Zhang J, Zhao H, Zhou G, Li J (2007) Analytical multi-scale method for multi-phase complex systems in process engineering–bridging reductionism and holism. Chem Eng Sci 62(13):3346–3377

Ge W, Li J (2002) Physical mapping of fluidization regimes—the EMMS approach. Chem Eng Sci 57:3993–4004

Ge W, Wang W, Yang N, Li JH, Kwauk M, Chen FG, Chen JH, Fang XJ, Guo L, He XF, Liu XH, Liu YN, Lu BN, Wang J, Wang JW, Wang LM, Wang XW, Xiong QG, Xu M, Deng LJ, Han YS, Hou CF, Hua LN, Huang WL, Li B, Li CX, Li F, Ren Y, Xu J, Zhang N, Zhang Y, Zhou GF, Zhou GZ (2011) Meso-scale oriented simulation towards virtual process engineering (VPE)-the EMMS paradigm. Chem Eng Sci 66(19):4426–4458

Gidaspow D (1994) Multiphase flow and fluidization: continuum and kinetic theory description. Academic, New York

Helland E, Occelli R, Tadrist L (2000) Numerical study of cluster formation in a gas-particle circulating fluidized bed. Powder Technol 110:210–221

Kwauk M, Li J (1996) Fluidization regimes. Powder Technol 87(3):193–202

Lanneau KP (1960) Gas solid contacting in fluidized beds. Trans Inst Chem Engrs 38:125

Li J (1987) Multiscale-modeling and method of energy minimization for particle-fluid two-phase flow. Ph.D, Institute of Chemical Metallurgy, Chinese Academy of Sciences

Li J, Chen A, Yan Z, Xu G, Zhang X (1993) Particle-fluid contacting in circulating fluidized beds. In: Avidan AA (ed) Preprint of the fourth international conference on circulating fluidized beds, Hidden Valley, pp 49–54

Li J, Cheng C, Zhang Z, Yuan J, Nemet A, Fett FN (1999) The EMMS model and its application, development and updated concepts. Chem Eng Sci 54:5409–5425

Li J, Kwauk M (1994) Particle-fluid two-phase flow: the energy-minimization multi-scale method. Metallurgical Industry Press, Beijing

Li J, Kwauk M (2001) Multi-scale nature of complex fluid-particles systems. Ind Eng Chem Res 40:4227–4237
Li J, Kwauk M (2003) Exploring complex systems in chemical engineering: the multi-scale methodology. Chem Eng Sci 58:521–535
Li J, Reh L, Kwauk M (1990) Application of the principle of energy minimization to fluid-dynamics of circulating fluidized bed. In: Basu P, Horio M, Hasatani M (eds) Circulating fluidized bed technology III. Pergamon Press, Oxford, pp 105–111
Li J, Reh L, Kwauk M (1992) Role of energy minimization in gas-solid fluidization. In: Potter OE, Nicklin DJ (eds) Fluidization VII. Engineering Foundation, New York, pp 83–91
Li J, Tung Y, Kwauk M (1988a) Axial voidage profiles of fast fluidized beds in different operating regions. In: Basu P, Large JF (eds) The 2nd international conference on circulating fluidized beds. Pergamon Press, Oxford, pp 193–203
Li J, Tung Y, Kwauk M (1988b) Multi-scale modeling and method of energy minimization in particle-fluid two-phase flow. In: Basu P, Large JF (eds) Circulating fluidized bed technology II. Pergamon Press, New York, pp 89–103
Li J, Zhang J, Ge W, Liu X (2004) Multi-scale methodology for complex systems. Chem Eng Sci 59:1687–1700
Li JH, Wen LX, Qian GH, Cui HP, Kwauk M, Schouten JC, Van Den Bleek CM (1996) Structure heterogeneity, regime multiplicity and nonlinear behavior in particle-fluid systems. Chem Eng Sci 51(11):2693–2698
Li Y, Kwauk M (1980) The dynamics of fast fluidization. In: Grace JR, Matsen JM (eds) Fluidization. Pergamon Press, New York, pp 537–544
Liu X, Gao S, Li J (2005) Characterizing particle clustering behavior by PDPA measurement for dilute gas-solid flow. Chem Eng J 108(3):193–202
Liu X, Gao S, Song W, Li J (2006) Effect of particle acceleration/deceleration on particle clustering behavior in dilute gas-solid flow. Chem Eng Sci 61:7087–7095
Liu XH, Li JH, Ge W (2011) A method to fast predict macro hydrodynamics of complex fluidization systems. China Patent 201110122298.X
Lu BN, Zhang N, Wang W, Li JH (2012) Extending EMMS-based models to CFB boiler applications. Particulogy 10(6):663–671
Matsen JM (1982) Mechanics of choking and entrainment. Powder Technol 32(1):21–33
Perry RH, Green DW (eds) (2007) Perry's chemical engineers' handbook. Mcgraw-Hill, New York
Reh L (1971) Fluidized bed processing. Chem Eng Prog 67(2):58–64
Reh L, Li JH (1991) Measurement of voidage in fluidized beds by optical probes. In: Basu P, Horio M, Hasatani M (eds) Circulating fluidized bed technology III. Pergamon Press, New York, pp 105–113
Romero JB, Johanson LN (1962) Factors affecting fluidized bed quality. Chem Eng Prog Symp Series 58:28–34
Shi ZS, Wang W, Li JH (2011) A bubble-based EMMS model for gas-solid bubbling fluidization. Chem Eng Sci 66(22):5541–5555
Wang W, Li J (2007) Simulation of gas-solid two-phase flow by a multi-scale CFD approach: extension of the EMMS model to the sub-grid scale level. Chem Eng Sci 62:208–231
Wang W, Lu B, Dong W, Li J (2008) Multi-scale CFD simulation of operating diagram for gas-solid risers. Can J Chem Eng 86(3):448–457
Wen CY, Yu YH (1966) Mechanics of fluidization. Chem Eng Prog Symp Series 62:100–111
Wilhelm RH, Kwauk M (1948) Fluidization of solid particles. Chem Eng Prog 44:201–207
Xu G, Li J (1998) Analytical solution of the energy-minimization multi-scale model for gas-solid two-phase flow. Chem Eng Sci 53(7):1349–1366
Yang N, Wang W, Ge W, Li J (2003) CFD simulation of concurrent-up gas-solid flow in circulating fluidized beds with structure-dependent drag coefficient. Chem Eng J 96:71–80
Yerushalmi J, Turner DH, Squires AM (1976) The fast fluidized bed. Ind Eng Chem Process Des Devel 15:47–53

Zhang DZ, Vanderheyden WB (2002) The effects of mesoscopic structures on the macroscopic momentum equations for two-phase flows. Int J Multiph Flow 28:805–822

Zhang J, Ge W, Li J (2005) Simulation of heterogeneous structures and analysis of energy consumption in particle-fluid systems with pseudo-particle modeling. Chem Eng Sci 60(11): 3091–3099

Zhang N, Lu B, Wang W, Li J (2008) Virtual experimentation through 3D full-loop simulation of a circulating fluidized bed. Particuology 6(6):529–539

http://www.springer.com/978-3-642-35188-4

From Multiscale Modeling to Meso-Science
A Chemical Engineering Perspective
Li, J.; Ge, W.; Wang, W.; Yang, N.; Liu, X.; Wang, L.; He, X.; Wang, X.; Wang, J.; Kwauk, M.
2013, XXVI, 484 p., Hardcover
ISBN: 978-3-642-35188-4